Acta Crystallographica Section B
Structural Science
ISSN 0108-7681

Structure solution of the basic decagonal Al–Co–Ni phase by the atomic surfaces modelling method

Antonio Cervellino,† Torsten Haibach and Walter Steurer*

Laboratory of Crystallography, Swiss Federal Institute of Technology (ETHZ) and University of Zurich, Zurich, Switzerland

† Present address: IRMEC-CNR c/o, Dipartimento Geomineralogica, Università di Bari, Via Orabona 4, I-70125 Bori, Italy.

Correspondence e-mail: steurer@kristall.erdw.ethz.ch

Received 11 June 2001
Accepted 7 November 2001

The atomic surfaces modelling technique has been used to solve the structure of the basic Ni-rich Al–Co–Ni decagonal phase. Formula $Al_{70.6}Co_{6.7}Ni_{22.7}$, space group $P\overline{10}$, five-dimensional unit-cell parameters: $d_1 = d_4 = 4.752$ (3) Å, $d_2 = d_3 = 3.360$ (2) Å, $d_5 = 8.1710$ (2) Å; $\alpha_{12} = \alpha_{34} = 69.295^\circ$, $\alpha_{13} = \alpha_{24} = 45^\circ$, $\alpha_{14} = 41.410^\circ$, $\alpha_{23} = \alpha_{i5} = 90^\circ$ (i = 1–4), V = 291.2 (7) Å^5; $D_x = 3.887$ Mg m^{-3}. Refinement based on $|F|$; 2767 unique reflections ($|F| > 0$), 749 parameters, $R = 0.17$, $wR = 0.06$. Describing the structure of quasicrystals embedded in n-dimensional superspace in principle takes advantage of n-dimensional periodicity to select the minimal set of degrees of freedom for the structure. The method of modelling of the atomic surfaces yielded the first fully detailed structure solution of this phase. Comparison with numerous former, less accurate models confirms several features already derived, but adds a new essential insight of the structure and its complexity. The atoms fill the space forming recurrent structure motifs, which we will (generically) refer to as clusters. However, no unique cluster exists, although differences are small. Each cluster shows a high degree of structural disorder. This gives rise to a large configurational entropy, as much as expected in a phase which is stable at high temperature. On the other side, the cluster spatial arrangement is perfectly quasiperiodic. These considerations, corroborated by analysis of the structural relationship with neighbouring periodic phases, strongly suggest the existence of a non-local, long-range interaction term in the total energy which may be essential to the stability.

1. Introduction

The identification (Zhang, 1995; Zhang, Estermann & Steurer, 1995) of the basic Ni-rich decagonal Al–Co–Ni phase has created widespread scientific interest and is a subject of intensive study. The detailed characterization of its complex structure is an enormous work and it has only been possible by collecting and comparing all the previous work, which we duly acknowledge throughout the paper. The atomic surface modelling technique (Cervellino, 2001) has been applied before to icosahedral Al–Cu–Fe (Katz & Gratias, 1994) and, very recently, to decagonal Al–Co–Ni (Takakura *et al.*, 2001), both based on rather small data sets. Applying the same technique, and using a large high-resolution synchrotron data set, we are able to present here a high-quality crystal structure solution.

A Copernican revolution in the understanding of quasiperiodic long-range order is underlined: all previous models

are based on the (regular or random) ordering of some well defined, ordered atomic cluster.[1] Although we can clarify the regularity of the disposition and confirm the existence of a basic atomic cluster, the nature of the latter is defined only as a statistical object. In fact, we find that the majority of atomic sites in such a cluster are only partially occupied; moreover, several slightly different variants of such a basic unit exist. In synthesis, we have a regular arrangement of irregular building blocks.

The plan of the paper is as follows. In the remainder of this section, we will present all the necessary background information, characterizing this quasicrystal in its phase diagram, in reciprocal space and in direct space. In §2 we describe the structure model we used and present the results of its refinement. §3 contains a comparative discussion of all previously issued structure models. §4 is dedicated, finally, to the discussion of the relation between the structure as solved and the stability of the decagonal phase.

1.1. The Al–Co–Ni system

A stable decagonal quasicrystal (*d*-QC hereafter) in the Al–Co–Ni system has been first identified by Tsai *et al.* (1989). The Al–Co–Ni phase diagram has successively been thoroughly explored (Gödecke & Ellner, 1996, 1997; Gödecke, 1997; Scheffer *et al.*, 1998; Gödecke *et al.*, 1998) and different *d* phases as well as periodic approximants have been found (see Zhang, 1995; Ritsch, 1996; Baumgarte *et al.*, 1997; Zhang *et al.*, 1997; Ritsch *et al.*, 1998, and references therein).

1.1.1. Quasicrystal-related Al-rich Al(Co,Ni) periodic phases. The relational analysis of QCs and approximants[2] is universally acknowledged as a key topic to understand quasiperiodicity. We introduce here a functional classification of periodic approximants to which we will refer in the following.

(i) Large-unit-cell (LUC) approximant phases: These are approximants in the strict sense (Steurer & Haibach, 1999*a*). They have been object of considerable study, in particular those with a large enough unit cell ($>400 \times c_{10}$ Å^3, c_{10} being the period along the pseudo-decagonal axis) to contain properly formed QC structure motifs, in particular 20 Å diameter decagons (broadly discussed later). In fact, these approximants form characteristic inflation series with increasing lattice parameters, tending asymptotically to the corresponding QC. They seem to be thermodynamically stable only at high temperature, grossly in the same range of QC, which is possibly the high-temperature thermodynamic equilibrium. In relation to *d*-Al–Co–Ni, known examples are $Al_{70}Co_{15}Ni_{15}$ (Grushko *et al.*, 1998; Estermann *et al.*, 2000; Lemster, 2001) and τ^2-$Al_{13}Co_4$ (Ma & Kuo, 1994; Ma *et al.*, 1995; Saitoh, Yokosawa *et al.*, 1999; Lemster, 2001). It is presently understood that they are structurally very similar to *d*-QC's of corresponding composition, up to hypothesizing crystal–QC reversible phase transitions. Intermediate stages of such phase transitions have been observed and their possible mechanism has been thoroughly discussed (Estermann *et al.*, 1994; Kalning *et al.*, 1994, 1995, 1997; Ritsch, 1996; Honal *et al.*, 1998; Steurer & Haibach, 1999*b*; Steurer, 1999*b*, 2000). However, high-quality structure solutions are not yet available, due to large disorder and sheer complexity. Therefore, we cannot presently use them for structure comparison.

(ii) Small unit-cell periodic phases with pentagonal motifs (PM phases): Several binary and ternary small unit-cell Al-rich phases ($V_{cell} < 400 \times c_{10}$ Å^3) are known which contain pentagonal atomic motifs, closely related to those in the *d* phases. However, there are also important structural differences, as will be discussed. The most important are $Al_{13}TM_4$, with TM = Co,(Co,Ni) or Fe (Hudd & Taylor, 1962; Grin *et al.*, 1994*a*; Freiburg *et al.*, 1996; Zhang, Gramlich & Steurer, 1995); $Al_{11}Co_4$ (Li, Shi *et al.*, 1995); Al_9Co_2Ni (Grin *et al.*, 1998); Al_5Co_2 (Burkhardt *et al.*, 1998; Yamamoto *et al.*, 1999). Comparative structural discussions about structure motif relations with *d*-Al–Co–Ni are found in Zhang (1995), Cockayne & Widom (1998*a*), Steurer (2001*b*) and Mihalkovič *et al.* (2001). Thermodynamically and chemically, PM phases differ from Ni-rich *d*-Al–Co–Ni. In fact, many PM phases are thermodynamically stable at ambient temperature; furthermore, in their composition nickel is minor or absent.

(iii) Small unit-cell *vacancy-ordered* periodic phases related to *d*-Al–Co–Ni as its *periodic average structure* (VOPAS phases). The concept of periodic average structure (PAS), which allows the inclusion of QCs in the world of incommensurately modulated structure, is explained in Steurer & Haibach (1999*b*), Steurer (1999*a*, 2000). Recently we have shown (Steurer & Cervellino, 2001) the importance of the QC–PAS relation in *d*-$Al_{70.6}Co_{6.7}Ni_{22.7}$. The PAS referred to as AS–2 in Steurer & Cervellino (2001) is the (CsCl type) β-phase AlNi. This phase accepts a large number of Ni-site vacancies, up to the composition $Al_{62}Ni_{38}$ (Bradley & Taylor, 1937*a*). Vacancy-ordering (VO) explains various superstructures (Al_4Ni_3, Ellner *et al.*, 1989; Al_3Ni_2, Dong, 1989). Notably, also, the surface of *d*-Al–Co–Ni transforms uniformly into the β-phase after ion irradiation (Zurkirch *et al.*, 1998).

1.1.2. Al–Co–Ni decagonal phases. Al–Co–Ni *d*-phases are periodic with a 4 Å period along the decagonal axis and quasiperiodic in planes orthogonal thereto. Structurally, there are two equispaced atomic layers per period.

d-Phases are found at 70–73 at.% Al, with 0–25 at.% Ni [*d*-$Al_{73}Co_{27}$ (Ma & Kuo, 1994; Saitoh *et al.*, 1994; Saitoh, Yokosawa *et al.* 1999) is only metastable]. It has been established (Zhang, 1995; Ritsch, 1996; Ritsch *et al.*, 1996; Zhang *et al.*, 1997; Baumgarte *et al.*, 1997) that at low Co content (6–8%) a *d*-phase exists, stable at high temperature (~1123–1323 K). It presents the simplest diffraction pattern (*basic d*-phase). Other *d*-phases, thermodynamically stable in lower temperature ranges (~973–1273 K, possibly less) and with a higher Co

[1] For reasons of conciseness, the term 'cluster' is used throughout this work with the generalized (and substantially geometric) meaning of 'structure motif' or 'quasi-unit-cell decoration' (Jeong & Steinhardt, 1997). In its usual, more restrictive, crystal-chemical acception, this term would not be justified because the inter-cluster and intra-cluster atomic bonds do not differ in any way.

[2] We employ this term in the broad meaning of 'periodic phases possessing chemical, physical and structural similarities with a QC'. A more restrictive definition is often used, based on lattice metrics (Steurer & Haibach, 1999*a*).

content, can be classified as its superstructures, the best characterized being the Edagawa phase (Edagawa *et al.*, 1992; Haibach *et al.*, 1999) at ~15 at.% Co. Other superstructures are found at higher Co content (Yamamoto *et al.*, 1990; Hiraga *et al.*, 1991; Steurer & Frey, 1993; Zhang, 1995; Ritsch, 1996; Ritsch *et al.*, 1998, 1999; Hiraga *et al.*, 2000). Enrichment in Co progressively lowers the structural symmetry.

All *d*-Al–Co–Ni phases show a fair amount of diffuse scattering. Especially noticeable are diffuse layers orthogonal to the tenfold axis with half-integer index. They appear very sharp in the tenfold axis direction, with coherence lengths superior to 300 Å (Steurer & Frey, 1993, 1998). The diffuse interlayers hint to a doubling of the translational period from 4 to 8 Å. In the basic phase this phenomenon is minimized and not apparently structured (Baumgarte *et al.*, 1997). Neither Bragg peaks nor structured diffuse phenomena can be observed in the half-integer diffuse layers; accordingly, the 8 Å superorder has to be of a simple (unidimensional) nature.

1.1.3. The basic Al–Co–Ni decagonal phase. The basic Ni-rich *d*-Al-Co-Ni phase has attracted considerable attention and many structure models have been proposed, without succeeding up until now in describing in detail its structure. In fact, its clean diffraction pattern, thermodynamic stability and the high attainable crystal quality have made it a benchmark of QC science. Hence, quite naturally, in our project of development of superspace-based methods for *d*-QC structure solution, basic *d*-Al–Co–Ni was chosen as the prototype for developing and testing the atomic surfaces (AS's hereafter) modelling technique (Cervellino, 2001). The structure determined here is only compatible with a simple 8 Å superstructure. The highlights of many former structure models are confirmed and explained, also clarifying some apparent contradictions. In addition, new important structural features have been found, which may help to shed some light on the still elusive phenomenon of quasiperiodic long-range order.

1.2. Reciprocal space analysis

A sample of good crystal quality and of suitable size for X-ray diffraction experiments was synthesized in our laboratory (see Baumgarte *et al.*, 1997; Zhang *et al.*, 1997, for details). The stoichiometric formula $Al_{70.6}Co_{6.7}Ni_{22.7}$ was determined by electron microprobe (CAMECA SX50, ±0.1 at.%). The sample was extensively characterized by X-ray photographic techniques, showing a decagonal diffraction pattern composed essentially of sharp Bragg peaks with a limited amount of interlayer diffuse scattering (Baumgarte *et al.*, 1997; Zhang *et al.*, 1997). This is a strong indication against a random tiling structure (see *Appendix* A2.2). To further assess the sample quality, two-dimensional grid scans (Haibach *et al.*, 2000) on sensitive Bragg peaks were performed at the six-circle diffractometer beamline at SNBL/ESRF. We could characterize the sample as a good single decagonal quasicrystal, excluding twinned approximants. The correlation length was $\simeq 1$ μm. The Bragg peak's HWHM does not increase at high $|\mathbf{q}|^{\perp}$, indicating the absence of phason strain (Abe, Matsuo *et al.*, 2000). The X-ray data collection was performed at the six-circle diffractometer beamline D3 at the synchrotron source Hasylab (DESY; Haibach *et al.*, 1995). 8404 reflections have been measured, each one with its profile to allow parabolic background correction. Profile integration yielded an expected R value, $R_\sigma = 0.0196$. Reflections were indexed in five-dimensional indices by the standard five-dimensional embedding (see Steurer & Haibach, 1999*a*, 2001; see also §1.3 and *Appendix* A1). Centroid statistics analysis (Haibach *et al.*, 2000) confirmed the exact correspondence with the five-dimensional embedding. The quasicrystal reciprocal metric constants[3] were determined as $a^* = 0.2662\,(1)$ and $c^* = 0.244768\,(6)$ Å^{-1} and the direct metric constants $a = 1/a^* = 3.757\,(2)$ Å and $c = 1/c^* = 4.0855\,(1)$ Å. c is the translation period along the tenfold axis. The superstructure translation period is $2c = 8.1710\,(2)$ Å.

Merging the data in the Laue group $10/m\,mm$ yielded 1544 unique reflections (internal R value $R_i = 0.029$, weighted internal R value $wR_i = 0.049$). A second merging in the Laue group $10/m$ yields 2767 unique reflections, with $R_i = 0.030$, $wR_i = 0.048$. Of the possible systematic absences, as listed in Rabson *et al.* (1991) or Steurer & Haibach (1999*a*), only the $0000h_5$: $h_5 = 2n + 1$ rule was strictly verified. The $h_1h_2h_2h_1h_5$: $h_5 = 2n + 1$ rule was consistently violated (95 unique reflections, 82 with $I > \sigma_I$); the $h_1h_2\overline{h}_2\overline{h}_1h_5$: $h_5 = 2n + 1$ rule was weakly violated (52 unique reflections, 19 with $I > \sigma_I$). It is almost equivalent to the selection of space groups $P10_5/mmc$ or $P10_5/m$. We kept the indication $P10_5/m$ in order to investigate the reason for this pseudosymmetry. The results (see §2.7 and deposited material[4]) indicate that the symmetry breaking is much more visible in $E^{\perp}$ (*i.e.* on the shape of the atomic surfaces) than in physical space, where its effect is lost in a maze of partly occupied atomic sites.

1.3. Patterson analysis

1.3.1. Interatomic vectors. The interatomic nearest-neighbour vectors have been determined by the Patterson map analysis (see Fig. 1). There are only two symmetry-inequivalent vectors in the (x_1, x_2) plane, $r_{\rm I}$ and $r_{\rm II}$ (as it happens in other *d*-QC's, see Cervellino *et al.*, 1998*a*, 2001*b*). The values are $r_{\rm I} = 2.45$ Å $\simeq a_r$, $r_{\rm II} = 2.85$ Å $\simeq \chi a_r$. We denote by $a_r \equiv 2\tau a/5$ an idealized bond length (see §A1). Their ratio is $\sim \chi = (3 - \tau)^{1/2} = 1.1755$ *etc*. The number we denote as $\chi = 2\sin(\pi/5)$ is the edge-to-radius ratio of a regular pentagon. The polar angles are $\alpha_{\rm I} = k\pi/5$, $\alpha_{\rm II} = \pi/10 + k\pi/5$. This geometry indicates a centred pentagon (or a fragment thereof) as the basic local atomic configuration.

1.3.2. Five-dimensional embedding. The n-dimensional embedding (Bak, 1985; Kalugin *et al.*, 1985; Duneau & Katz, 1985; Janssen, 1986) is a well established method for describing quasiperiodic patterns. We embed *d*-QC's in a five-

[3] a^* and c^* are defined (Steurer *et al.*, 1993; Steurer & Haibach, 1999*a*, 2001) as the physical reciprocal space lengths of the (10000) and (00001) reflections in the standard embedding, respectively.

[4] Supplementary data for this paper are available from the IUCr electronic archives (Reference: SN0016). Services for accessing these data are described at the back of the journal.

Table 1
Experimental details.

Crystal data	
Chemical formula	$Al_{70.6}Co_{6.7}Ni_{22.7}$
Chemical formula weight	3632.11
Cell setting, space group	Decagonal, $P\overline{1}0$
d_1, d_2, d_3, d_4 (Å)	4.752 (3), 3.360 (2), 3.360 (2), 4.752 (3)
$d_5 \equiv c$ (Å)	4.0855 (1) (average 4 Å structure)
$d_5 \equiv 2c$ (Å)	8.1710 (2) (8 Å superstructure)
α_{12}, α_{13}, α_{14}, α_{23}, α_{24}, α_{34} (°)	69.295, 45, 41.410, 90, 45, 69.295
α_{i5} (°, i = 1,...4)	90
V (Å^5)	291.2 (7)
D_x (Mg m^{-3})	3.887
D_{meas} (Mg m^{-3})	3.94 ± 1%, for Co 8 at.% (Steinhardt *et al.*, 1998; Saitoh *et al.*, 1998; Abe, Saitoh *et al.*, 2000) 4.186 ± 0.8%; 4.2, for Co 13–15 at.% (Chernikov *et al.*, 1998; Nakao *et al.*, 1992; Steurer *et al.*, 1993)
Radiation type	Synchrotron
Wavelength (Å)	0.53905
No. of reflections for cell parameters	20
θ range (°)	1.5–65.0
μ (mm^{-1})	5.2882
Temperature (K)	298
Crystal form	Decaprismatic
Crystal size (mm)	0.31 × 0.31 × 0.95
Data collection	
Diffractometer	Huber four-circle, beamline D3, HASYLAB
Data collection method	ω scans
Absorption correction	Analytical
No. of measured reflections	8404
No. of independent reflections	2767
No. of observed reflections	2767
Criterion for observed reflections	$I > 0$
θ_{max} (°)	65.0
No. of standard reflections	2
Frequency of standard reflections	Every 45 min
Intensity decay (%)	0
Intensity fluctuation (r.m.s. %)	2.03

dimensional space E (Steurer, 1990; Steurer & Haibach, 1999*a*, 2001). Some details are recalled in §A1.

After performing the data reduction in the standard five-dimensional embedding (Steurer & Haibach, 1999*a*, 2001) we performed a Patterson embedding analysis (Cervellino, 2001; Cervellino *et al.*, 1998*a,b*). The procedure we employed is based on the determination of the strongest family of maxima on the quasiperiodic plane E^Q of the Patterson function, which is the electron density autocorrelation. The five-dimensional lattice parameters have been redetermined (see Table 1) as those of the τ^{-1} embedding (Cervellino *et al.*, 1998*a*). This yields the most convenient unit-cell geometry in n-dimensional superspace. At the same time, this corresponds to a correlation analysis in physical space, allowing for the identification of the scale and distribution of structural motifs (tiles or covering clusters), as in the next section.

1.3.3. Tiling correlation analysis. Tilings (or coverings) are often used to describe the physical space structure of QCs. Some theoretical notions are recalled in §A2. A tiling is understood as a space covering (with or without overlap) by a finite number of geometric objects (tiles) whose disposition follows a specific rule. Tile(s) are the analogue of the unit cell in a three-dimensional periodic crystal. The atomic decoration of the tiles will be dealt with later. Now we consider the rule of covering, because it is important to establish if this rule is deterministic or random (see §A2.2). Patterson analysis confirms, as the diffraction pattern qualitatively indicates, perfect quasiperiodicity.

Joseph *et al.* (1997) proposed a method to decide if a tiling is perfectly quasiperiodic or random. The method is based on visual recognition from electron density images of a basic cluster, followed by reporting the cluster centre coordinates in five-dimensional space. Another procedure is possible, which eliminates the arbitrariness implicit in the visual recognition. The Patterson function P is the electron density autocorrelation. The vectors between the most frequent structure motifs correspond to very high correlation values. Of particular interest is the $(000x_4x_5)$ section around the origin. The Patterson function on this section will be the autoconvolution of the AS which define the cluster centres (working in terms of a PPT or GDC, see §A2 for details). The deconvolution is still an awkward problem, but important indications can be extracted nonetheless. Fig. 2 shows the Patterson profiles along $x4$ and $x5$. Filled circles mark the I^{obs} Patterson (I^{obs}_{00000} from the structure solution). Light-grey shading represents the calculated autoconvolution of the AS defining the vertices of a PPT[1]. The PPT[1] is the basic framework of a GDC[3], the latter consisting of the former's projected Voronoi clusters

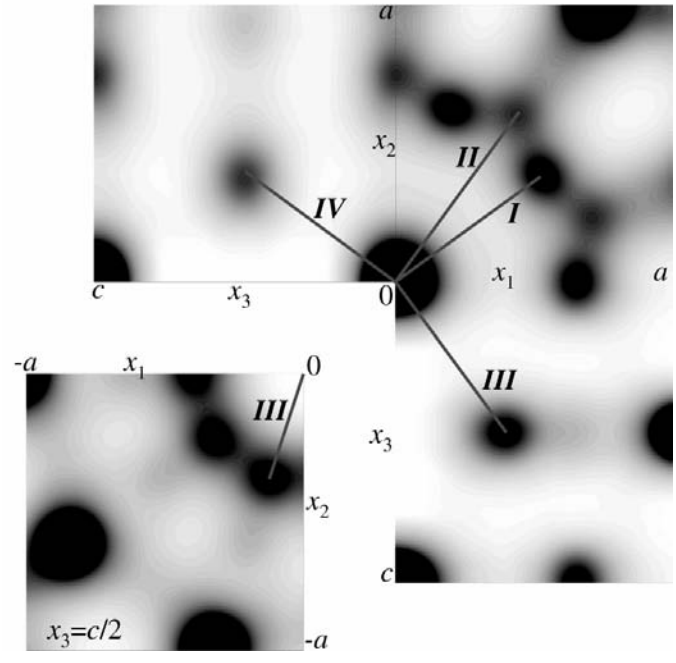

Figure 1
Patterson map sections near the origin for the interatomic distance determinations. In the $(x_1, x_2, 0)$ section peaks corresponding to the distances $r_I \simeq a_g = 2.43$ Å and $r_{II} \simeq 2.86$ Å are clearly visible, and no other peaks under 3 Å exist. In the $(x_1, 0, x_3)$ and $(0, x_2, x_3)$ sections other peaks (III and IV, respectively) can be seen; $r_{III} \simeq r_{IV} \simeq 2.53$ Å. The $(x_1, x_2, c/2)$ section shows that peak IV is the extension of III.

(Gummelt, 1996; Kramer, 1999). The GDC[3] is the same pattern of decagonal clusters of radius $\tau^3 a_r$ = 10.300 Å identified in all electron microscopy works following Steinhardt *et al.* (1998). The centres of the GDC[3] are in turn (Gummelt & Bandt, 2000) the vertices of a PPT[3] (*i.e.* a τ^2-inflated PPT[1]). Their autoconvolution is also represented (dark-grey shade). The PPT[1] autoconvolution fits well the data; however, a residual misfit (shown as the difference-Patterson profile, dotted line) is present. Can this be an indication of a significant randomization of the basic tiling? Two other difference-Patterson profiles have been calculated to address the question. Continuous line: a simple modification of the geometry of the AS (see Niizeki, 1993). The misfit is significantly reduced. Dashed line: the addition of a large phasonic thermal factor (four times the overall value determined for the atomic structure) causes a much larger misfit. We can conclude, confirming the result of Joseph *et al.* (1997) and Hory *et al.* (1999), that a random tiling does not describe this *d*-QC. However, its basic tiling is more complex than a Penrose tiling.

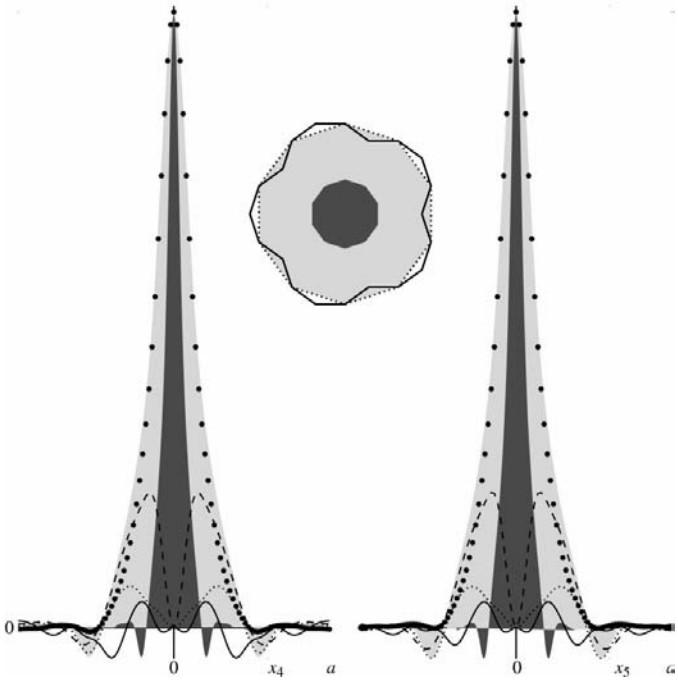

Figure 2
Patterson sections in perpendicular space can verify the existence and the scale of an ideal tiling. Left: section along x_4, centred on the origin; right: section along x_5, centred on the origin. *Black circles*: the Patterson function of the QC, calculated from the observed intensities ($I_{(00000)}$ taken from the structure solution). All compared curves have been scaled to have the same value in the origin. *Dark grey shaded profile*: the calculated autocorrelation of a Penrose pentagonal tiling PPT[3], describing the centres of a 20 Å diameter decagon (Gummelt, 1996; Jeong & Steinhardt, 1997; Steinhardt *et al.*, 1998). The relevant AS is drawn in the centre of the figure (*dark grey decagon*). (*a*) The scale of all AS's is doubled with respect to the rest of the figure; (*b*) for all the calculated profiles, the resolution has been equalized to the experimental one simply by calculating the diffracted intensity in the Bragg peaks positions of the QC's in reciprocal space. *Pale grey shaded profile*: the calculated autocorrelation of a Penrose pentagonal tiling PPT[1] (pentagon edge 4.625 Å). It agrees remarkably well with the calculated values; the difference profile is also reported (*dotted line*). The AS is shown in the centre of the figure (*pale grey decagon*). *Continuous line*: difference profile of the autocorrelation of a Penrose pentagonal tiling PPT[1] with a slight modification due to Niizeki (1993). The AS is shown in the centre of the figure (*starred decagon, continuous line*). Clearly, this modified tiling offers a better agreement; more complex modifications – beyond our scope – could yield further improvements. Also, the effect of slightly variable atomic decoration of the tiles (see text) should be taken into account. *Dashed line*: difference profile obtained by adding a large phasonic thermal factor to a basic Penrose pentagonal tiling (four times the refined value for *d*-$Al_{70.6}Co_{6.7}Ni_{22.7}$). The difference on the tails is not much recovered, needing a larger phasonic thermal factor; however, the difference in the central part is already very large. A significant random tiling contribution seems out of the question.

1.3.4. Atomic surfaces location. Another extremely useful result of Patterson analysis is the determination of the position and chemical composition of the centre of the AS's. The notation is explained in §A1.

Recall now that we have two atomic layers per *c*-period (for the 4 Å average structure). The x_3 coordinates of the two atomic layers are $c/4$, $3c/4$, so $z = 1/4, 3/4$. The Patterson function on the (**D**, **Z**) Harker section can be calculated (see Fig. 3) and deconvoluted by the Symmetry-Minimum/Image-seeking Minimum Function method, allowing for the determination of the AS's centres and their chemical composition. The technique has been described in Haibach & Steurer (1996) and applied to *d*-$Al_{70.6}Co_{6.7}Ni_{22.7}$ in Haibach *et al.* (1998). Two independent AS's resulted, AS **A** in $(q, z) = (1, 1/4)$, with TM core, and AS **B** in $(q, z) = (2, 1/4)$, with an Al core. In the $z = 3/4$ atomic layer there are two (10_5-related) inverted copies, **A**′ in $(q, z) = (4, 3/4)$ and **B**′ in

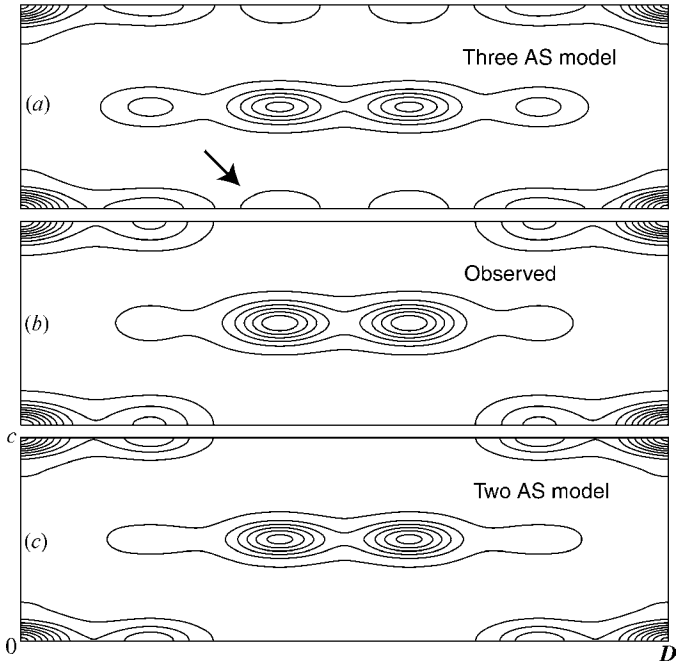

Figure 3
The Patterson function on the (**D**, **Z**) Harker section. (*a*) (top) shows the effect of introducing AS **C** as carved out from the centre of AS **B** (see §1.3.5). The arrows point to the additional peaks created by this supplementary AS. For comparison, (*b*) (centre) shows the I^{obs} Patterson; (*c*) (bottom) shows the I^{cal} Patterson calculated from our model, without the AS **C**, at the same refinement stage.

$(q, z) = (3, 3/4)$. The QC space group $P10_5/m$ forces these AS's to have symmetry 5 (while $P10_5/m\,mc$ would force symmetry $5m$).

The 8 Å superstructure has twice as many atomic layers and it will have two more AS pairs, at $z = 5/4$ and $z = 7/4$ (keeping the notation as in the average structure, for simplicity). The configuration of these two additional layers could be the same as the former two or an isometric one. We will consider the same configuration, for reasons that will be clarified in the next section.

1.3.5. Model selection. Many models have been proposed for our QC, the majority of which assumes (more or less explicitly) the same AS configuration as we do. There are, however, two classes of models which assume a different configuration. The Patterson analysis allows us to discard them without having to carry out a full comparative refinement.

The Al–Co–Cu *d*-QC is similar in many aspects to Al–Co–Ni, but it also has large differences. In some works (Burkov, 1991; Wittmann, 1999) the two structures are considered to be identical, apart from the obvious chemical substitutions. This identification is, at least, very approximate. In fact, the best current models of *d*-Al–Co–Cu (Steurer & Kuo, 1990; Li, Steurer *et al.*, 1995; Cockayne & Widom, 1998*b*) are built upon three AS's per atomic layer. The third one, AS **C**, is in $(q, z) = (3, 1/4)$ [and the related AS **C**′ in $(q, z) = (2, 3/4)$]. **C** is the centre of our **B**, carved out and translated by 1/5 along **D**. It is simple to show that this configuration is not isometric to that with two AS's. Fig. 3 shows clearly that the difference is quantitative. We used our structure model for the comparison, at an intermediate refinement stage. We modified the model introducing AS's **C**, **C**′. We calculated structure factors and from their squared moduli the Patterson function on the (**D**, **Z**) Harker section (Fig. 3). For comparison, the $I^{\rm obs}$ Patterson and the Patterson calculated from our model at the same refinement stage are also shown. It is evident that Al–Co–Cu/Al–Co–Ni cannot be considered to be fully isostructural.

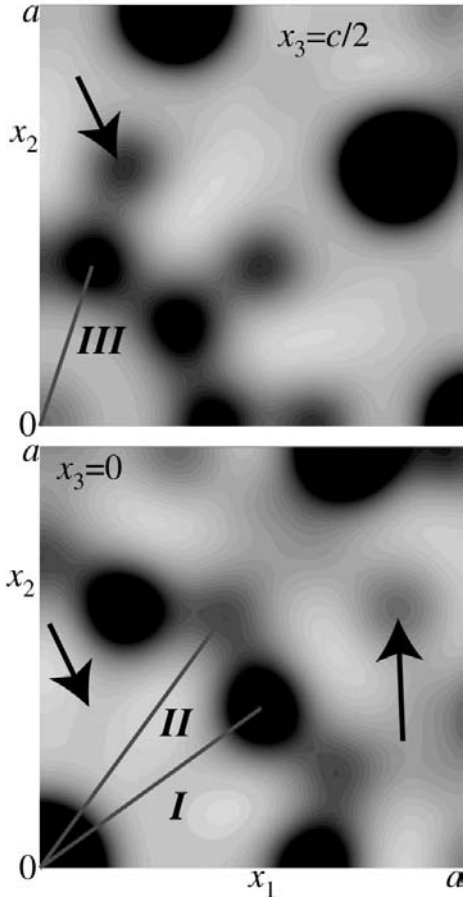

Figure 4
Patterson map sections near the origin for the $Al_{13}Co_4$-like 8 Å superstructure model (see §1.3.5). In both the $(x_1, x_2, 0)$ and the $(x_1, x_2, c/2)$ sections there additional interatomic peaks appear (indicated by arrows), which are nonexistent in the $I^{\rm obs}$ Patterson (*cf.* Fig. 1).

Another different AS configuration sometimes proposed for *d*-QC's in the Al–Co–Ni system regards the 8 Å (super)-structure with a configuration mutuated from the analysis of Al–Co or Al–Fe PM phases. These works (Yamamoto *et al.*, 1990; Cockayne & Widom, 1998*a*) regard, anyhow, very Co-rich or binary Al–Co *d*-phases, with strong differences in the diffraction pattern with respect to $Al_{70.6}Co_{6.7}Ni_{22.7}$. Differences in Co–Ni partition have marked structural effects. We will show that this AS configuration does not apply to $Al_{70.6}Co_{6.7}Ni_{22.7}$.

In our superstructure configuration, we have, in layer order: AS $\mathbf{A} \equiv (1, 1/4)$, AS $\mathbf{B} \equiv (2, 1/4)$; AS $\mathbf{A}' \equiv (4, 3/4)$, AS $\mathbf{B}' \equiv (3, 3/4)$; AS $\mathbf{A} \equiv (1, 5/4)$, AS $\mathbf{B} \equiv (2, 5/4)$; AS $\mathbf{A}' \equiv (4, 7/4)$, AS $\mathbf{B}' \equiv (3, 7/4)$. For simplicity, let us consider equal AS's with the same symbol, the prime marking a $\pi/5$ rotation. AS **A** contains most TM, while AS **B** is mostly Al. The alternative model differs only in the fourth layer, where we have a pair AS $\mathbf{A}' \equiv (4, 7/4)$, AS $\mathbf{B}' \equiv (0, 7/4)$. This corresponds to a $\pi/5$ rotation of all vectors between atom pairs generated by the two AS's at a distance of $a_r \simeq 2.4$ Å; in particular, several TM-centred Al pentagons of such radius are $\pi/5$ rotated.

First of all, we notice that this alternative configuration breaks the 10_5 screw symmetry. Therefore, consistent violations of the strong extinction rule $0000h_5$: $h_5 = 2n + 1$ (*cf.* §1.2) would be expected. In fact, this happens for the *d*-QC of Yamamoto *et al.* (1990).

This alternative configuration is isometric with respect to the (**D**, **Z**) Harker section. However, new interatomic vectors appear in the physical space sections (see Fig. 4). This is due to the coherent superposition, in the 4 Å average structure, of the second and fourth layer, so generating a decagon from two overlapped, inverted pentagons. The calculation has been carried out by a similar procedure as described before, at a more advanced refinement stage. Fig. 4 shows $(xy0)$ and $(xy\frac{1}{2})$ Patterson map sections, easily compared with Fig. 1. The appearance of artificial peaks is a concrete reason for discarding the alternative configuration and the models which contain it, at least regarding the Ni-rich composition. For very Co-rich *d*-Al–Co–Ni phases, as well as for intermediate compositions, a similar investigation would surely be interesting.

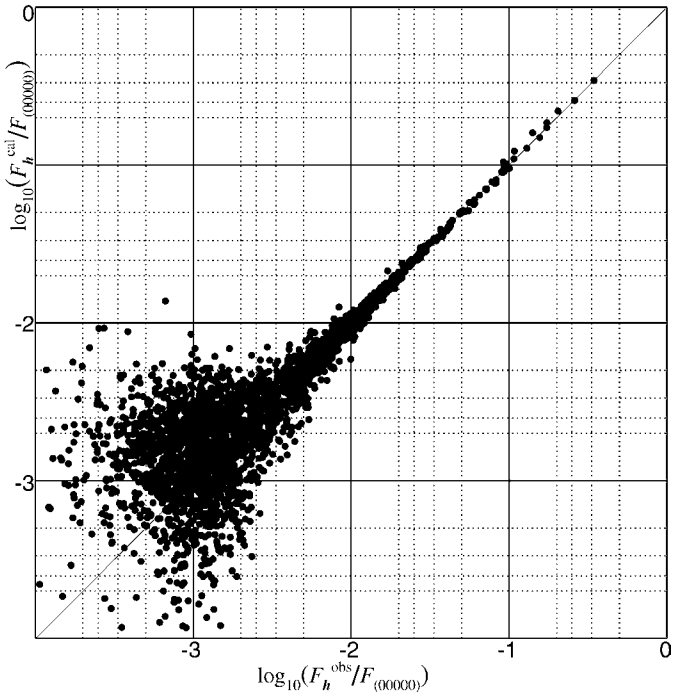

(*a*)

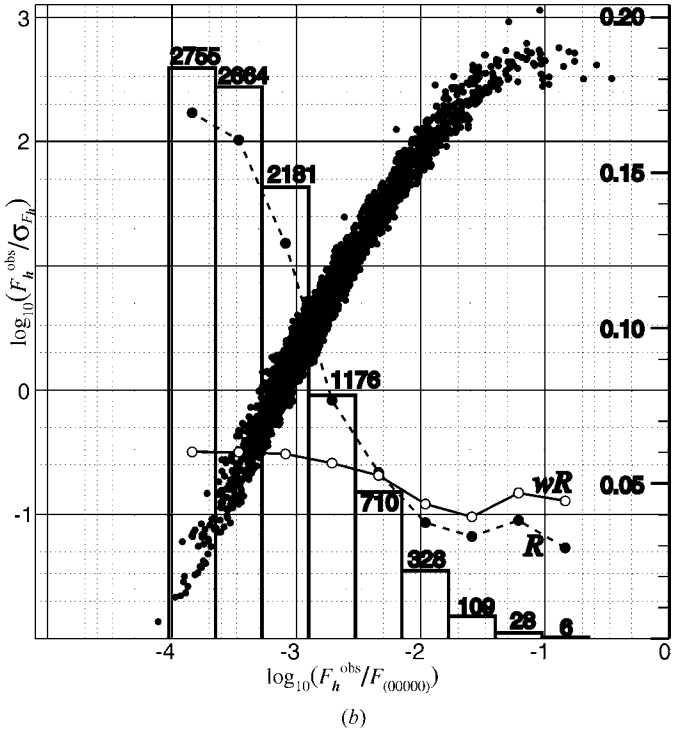

(*b*)

Figure 5
(*a*) Logarithmic $F_{\mathbf{h}}^{\rm cal}$ *versus* $F_{\mathbf{h}}^{\rm obs}$ plot of the structure refinement. $F_{(00000)}^{\rm cal}$ has been taken as unity. (*b*) Illustration of the weighting scheme and of the final error distribution. *Black dots*: logarithmic $F_{\mathbf{h}}^{\rm obs}/\sigma_{F_{\mathbf{h}}}$ *versus* $F_{\mathbf{h}}^{\rm obs}/F_{(00000)}^{\rm cal}$ plot to show the distribution of errors on the measured intensity. *Columns with numbers*: number of reflections over a given F threshold. Every column has a height proportional to the number of reflections with $F_{\mathbf{h}}^{\rm obs} > kF_{(00000)}^{\rm cal}$, where k is the centre of the column base (logarithmic scale). *Full circles, dashed line, right scale*: the unweighted agreement factor R calculated for each of the reflection subsets indicated by the corresponding column. *Empty circles, continuous line, right scale*: the weighted agreement factor wR calculated for the same reflection subsets.

2. Model and refinement

2.1. Atomic surface modelling

Here we sketch briefly the techniques we used to model the AS's. More details are given in Cervellino (2001). In principle, modelling the AS's is equivalent to building a model in which the properties of each atomic site are determined by its coordination polyhedra.

2.2. AS models for ideal quasicrystals

§A1 describes the concept of atomic surface in a probabilistic sense. This generalization has been introduced to allow for occupational disorder. At the beginning of our investigation, we did not consider fractional occupancy. We tried to model in terms of *ideal* structure, with all atomic sites occupied and fulfilling the *closeness condition* (Kalugin & Levitov, 1989; Katz & Gratias, 1994; Deus, 1995; Cervellino, 2001). This, loosely, requires the QC to be a Delone set of parameters $r_{\rm I}$ = 2.45, $r_{\rm II}$ = 2.85 Å (see §1.3.1), with at most one atom in any ball of radius $r_{\rm I}$ and at least two atoms in any ball of radius $r_{\rm II}$. The values of $r_{\rm I}$ and $r_{\rm II}$ were desumed from general crystal-chemical knowledge and from the Patterson map analysis (see §1.3.1). This requirement would also give a high mass and point density, around 4.5 Mg m^{-3} and 0.075 at. Å^{-3}. The resulting models, however, never compared well with the data; we obtained, with the most favourable geometries, $wR > 0.3$, which is not to be taken into consideration.

The main reason for this failure was addressed in the excessive density of such models. Measured mass densities for basic Ni-rich *d*-Al–Co–Ni are under 4 Mg m^{-3} (Table 1). In structural terms, the distance $r_{\rm I} \simeq 2.4$ Å is surely appropriate for TM–TM and Al–TM pairs, not so for Al–Al pairs, for which the distance $r_{\rm II} \simeq 2.8$ Å (as in pure Al; Ashcroft & Mermin, 1976*a*; Villars & Calvert, 1991) is more appropriate. This is not to be thought of as a rigid constraint – Al–Al pair distances ∼2.6 Å are found in Al–(Ni,Co) PM phases, but in a *small minority* of cases. In the ideal QC, Al–Al pairs at 2.4 Å would occur in a *large fraction* of cases (Cervellino *et al.*, 2000), which might be energetically unfavourable (see §2.6.1).

We briefly mention here another method for modelling the atomic surfaces (Burkov, 1993; Yamamoto, 1996), which we also tested with deluding results. The partition of the AS's can be appositely chosen so as to obtain equal atomic decoration of equivalent tiles of a (suitably chosen) tiling. This minimizes the structure model's degrees of freedom, making it easier to build and to interpret. However, there is no reason for this to be more than a crude approximation, as results show. From the physical point of view, the *ansatz* of 'equal decoration' corresponds to assume that (perfect) local ordering is prioritary over long-range ordering. This is the exact opposite of our findings, as this structure shows, first and foremost, long-range order, while local order is mostly statistical.

2.3. AS models for real quasicrystals

Introducing partial occupancy of the atomic sites or non-unity probability density on the AS's, has important consequences.

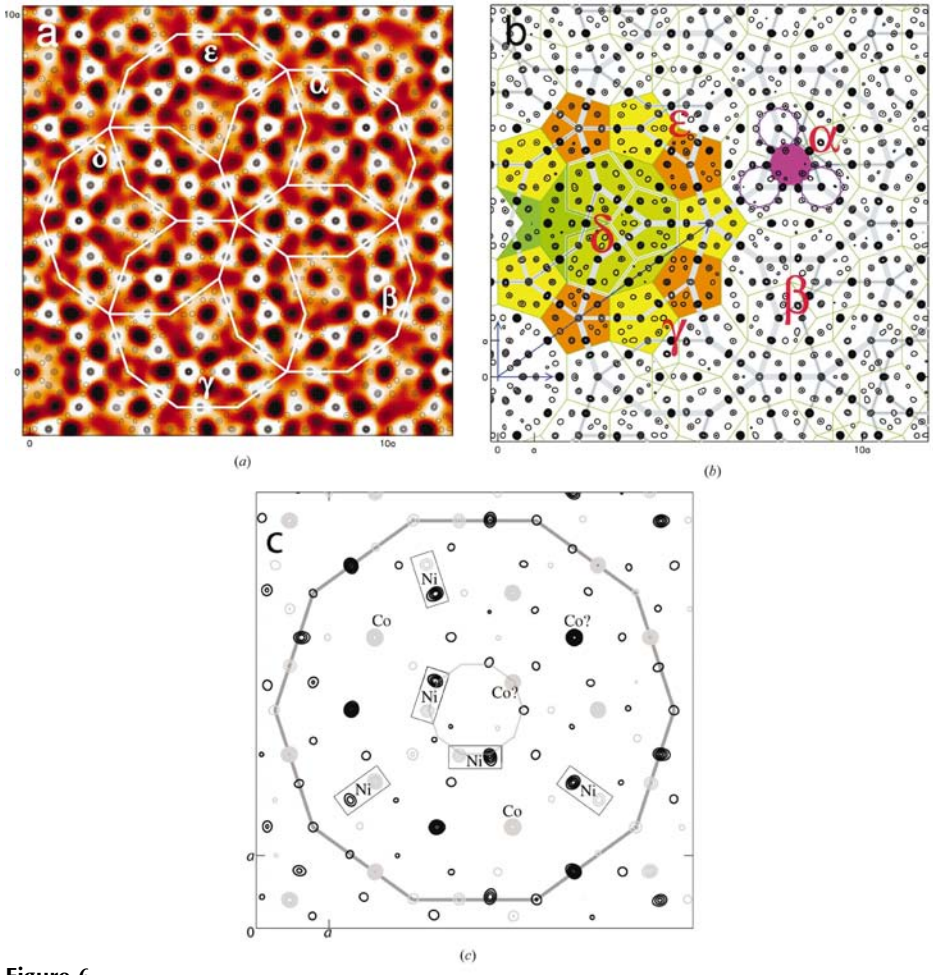

Figure 6
(*a*) *Red color scale map*: the projected electron density on the (x_1, x_2) plane at a resolution of 1 Å. Black is zero, white is maximum. *Black contour lines, overlaid*: the projected electron density at full resolution (0.15 Å). Contour lines every 10%. *Decagons*: a group of five Gummelt decagonal clusters, labeled by greek letters. Note that the centres of the clusters α, γ, δ appear clearly asymmetric, while clusters β, ϵ appear approximately decagonal. Compare with the EM images of Yan *et al.* (1998). (*b*) *Black contour lines*: the projected electron density (full resolution) on (x_1, x_2). *Green lines*: a pentagonal tiling (Niizeki's modification of a Penrose tiling, see text). This modified tiling better matches the projected motifs than the basic Penrose tiling, even if the correspondence is not yet perfect. All the intervertex vectors with length $\tau\chi a_r = 4.625$ Å are plotted. Note the characteristic tiles: pentagons, stars, boats and thin rhombi. As a rule, pentagons are decorated by a centred atomic decagon, while the other tiles are decorated by linear atomic motifs. *Grey lines*: network of Gummelt overlapping decagonal clusters, centred on a τ^2-inflated version of the pentagonal tiling. The five decagons marked with greek letters in the centre are the same as in (*a*). Note the Y configuration of three pentagons in the centre of each decagon; on their intersection an atomic decagon with an empty centre is formed. On cluster α this configuration is evidenced by pink motifs. Each decagon corresponds to a pair of inverted pentagons belonging to different atomic layers. *Green decagon, yellow/orange pentagons on cluster* δ: the double tiling introduced by Hiraga *et al.* (1994) and Yamamoto (1996). The green star corresponds to the 'ejection' of the tenth surrounded pentagon observed by Hiraga. The tile symmetry should match the decoration's symmetry; this is not the case. On clusters β and ϵ this is less evident. (*c*) Detail (cluster α) showing the TM contribution to the electron density; contour lines (10, 20,...90%). Black: contribution of the flat (F^+, F^-) layers; grey: contribution of the puckered ($P^\uparrow$, $P^\downarrow$) layers. Close TM pairs (< 3 Å) are marked as Ni atoms, isolated TM atoms are marked as Co, in agreement with EXAFS results (Zaharko *et al.*, 2001). In many cases partial site occupancy does not allow a clear distinction.

First of all, the crystal density and stoichiometry are now decoupled from the AS's geometry. This gives new degrees of freedom, with the possibility to introduce constraints so as to reproduce experimentally known values.

Secondly, configurational entropy is introduced in a natural way into the stucture. We recall that a high degree of configurational entropy is to be expected in phases whose range of thermodynamical stability is around 1273 K. This configurational entropy is achieved without having to introduce *ad hoc* a random tiling.

Thirdly, a structure derived from an AS model with non-unity probability would have a diffraction pattern composed mainly of Bragg peaks plus a smooth or constant diffuse background, as it is experimentally found for the majority of well ordered QCs. This diffractive behaviour has been rigorously demonstrated by Baake & Moody (1998), while it is not demonstrated (see §A2.2) that random tilings could produce any Bragg peak. Furthermore, as we already pointed out (Cervellino *et al.*, 2000; Haibach *et al.*, 2000; Steurer & Cervellino, 2001), many other desirable properties of AS models (robustness of parametrization, inflation symmetry, average periodic structure, existence of families of dense net planes orthogonal to all strong reflections) are still valid.

Finally, most short distance restraints can be removed or weakened. It is in fact possible to allow for very short intersite distances, provided that the relevant site occupancies are reasonably low. It is also implied as a natural way to introduce chemical disorder in the crystal model. Any atomic site may have different occupancies for different atomic species, provided that the sum does not exceed one.

All these arguments make the AS modeling technique an efficient, elastic and realistic tool for QC structure determination. Now we will show how we did build our model for basic Al–Co–Ni.

2.4. Projected structure

The first natural step was to build a model for the projected structure. As

many atomic distance restraints are weakened, we could start with very large AS's. These were derived from the shapes of the deterministic model presented in Cervellino *et al.* (2000). More extended and simpler shapes (pentagonal stars of radius $2\tau a/5$) have been chosen in order to explore thoroughly perpendicular space and to have a simple partition. They were subdivided in subregions by an appropriate mesh (Cervellino *et al.*, 2001*a*). The subdivision must of course be compatible with the AS's symmetry (given by the site symmetry at its centre, in our case 5). As outlined in Cervellino *et al.* (2000, 2001*a*) and Cervellino (2001), the mesh must contain all significant partition lines which identify atoms in a different local environment. This can be obtained by examining the overlap of neighbouring AS's whose centres lie within a fixed physical space distance from that under construction. This must be repeated for every physical space distance corresponding to an important coordination shell. Once a first partition is obtained the procedure can be iterated starting from the pre-partitioned AS's. Ideally, one iterates until no new partition line can be added; practically, one may stop well before that point, depending on the number of parameters to refine.

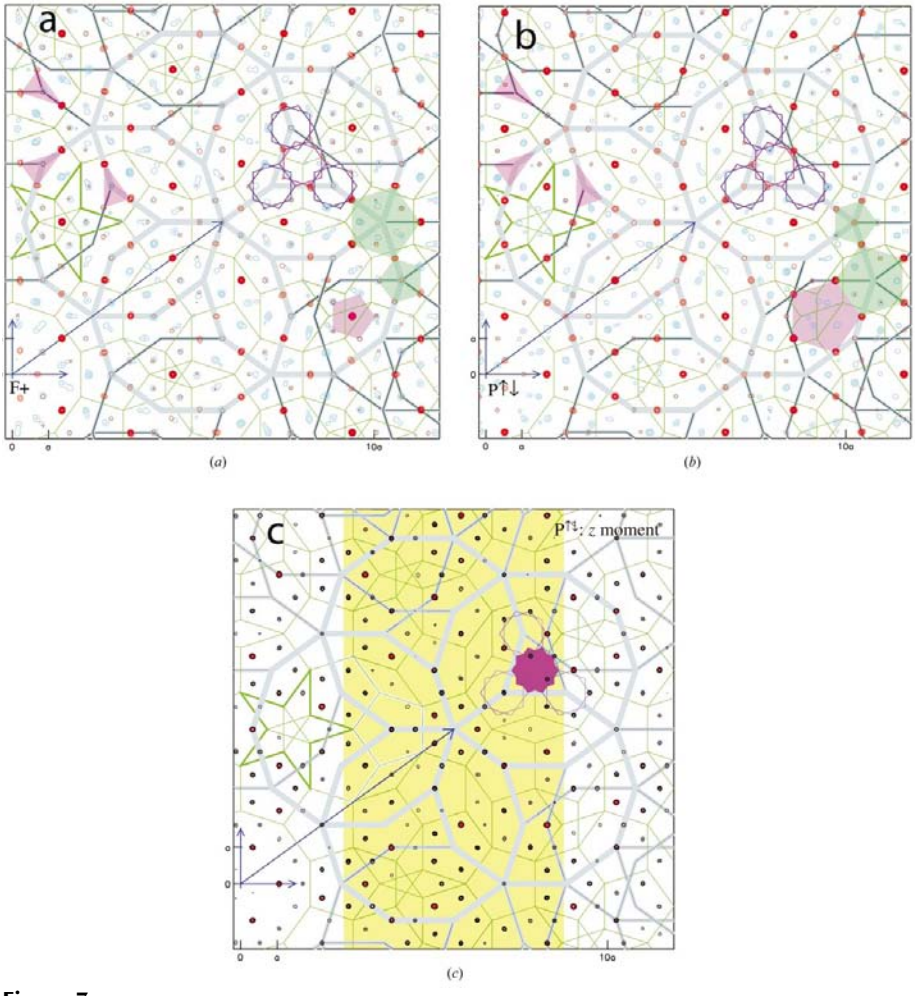

Figure 7
(*a*) The electron density on layer F^+ at $x_3 = c/4$. To allow uniform interpretation of flat and puckered layers, in all layers the electron density has been projected along x_3 on a thickness of ± 1 Å above and below each layer. The geometric motifs are the same as in Fig. 6(*b*). Separate contributions to the electron density are plotted (*red contour lines*, TM contribution; *blue contour lines*, Al contribution). The contours of TM electron density are every 10%; those for the Al density have been scaled by $Z_{Al}/Z_{Ni} = 13/28$ to give them the same evidence. On the left-hand side, *pink-shaded triangles* evidence some pentagonal atomic motifs; on the right-hand side, *colour-shaded pentagons* evidence pseudo-PBPs in differently phased configurations. (*b*) The electron density on layers $P^\uparrow$ ($P^\downarrow$) at $x_3 = 3c/4(7c/4)$. Same description. The average electron density of these layers is not much different from layer F^+, while layer F^- (not shown) is 10% less dense, although not dissimilar from F^+. *Pink triangles* and *colour-shaded pentagons* evidence the same structure motifs as in (*a*). (*c*) The x_3 moment of the electron density on the puckered layers. This shows the effect of puckering. Atoms lying exactly on the layer plane disappear, while atoms out-of-plane are evidenced. Black contour lines (10–40%) and red contour lines (50–100%) have been used to evidence the most shifted atoms. The yellow band identifies the parallelepiped whose bounded-projection along x_2 is shown in Fig. 8.

Every subregion is then assigned one or more chemical species, depending on some prior knowledge (see §1.3.4). Possible refinement parameters for every symmetry-unique subregion are probability (occupancy) and all static and dynamic atomic displacement parameters (ADPs). Global parameters (extinction, scale factor) must be added. When refining the projected structure, of course, all the z components of ADPs can be neglected. The dynamic ADP components in the (x_1, x_2) plane were assumed to be isotropic. As only reflections with $h_5 = 0$ are to be used, the parameters-to-observations ratio is very high, so it is important to keep free only those parameters which really influence the outcome; this means keeping the calculations under tight control.

At the beginning of the refinement, it is convenient to constrain density and stoichiometry to known or plausible values, otherwise calculation times become unacceptable and false solutions might be found. In our case the stoichiometry was precisely measured, but literature density values for similar composition were used (Steinhardt *et al.*, 1998; Saitoh *et al.*, 1998; Abe, Saitoh *et al.*, 2000). The density constraint was released at the last refinement cycles, resulting in a stable value.

At intermediate refinement stages it is possible to eliminate subregions which stabilize as empty. Once the statistical indicators were reasonably good ($wR < 0.12$) we used Fourier difference maps to decide slight modifications in the mesh geometry. The projected structure refinement ended with $wR = 0.028$ (471 reflec-

Table 2
Refinement details.

Refinement	
Refinement on	F
R	0.1701 (all 2767 unique reflections) 0.0777 ($I > 3\sigma_I$, 1198 unique reflections) 0.0599 ($I > 10^{-4}I_{max}$, 837 unique reflections)
wR	0.0601 (all 2767 unique reflections) 0.0568 ($I > 3\sigma_I$, 1198 unique reflections) 0.0542 ($I > 10^{-4}I_{max}$, 837 unique reflections)
S	11.46
$\|\Delta\rho\|_{max}$ (e Å^3)	1.97
$\|\Delta\rho\|_{max}$ (e per atom)	< 0.8
No. of reflections used in refinement	2767
No. of parameters	749
Weighting scheme	$w = 1/\sigma_F^2$
Extinction method	Becker–Coppens, Thornley, modified (see §2.6.1)
Extinction coefficient	0.75 (3) × 10^{-4}
Source of atomic scattering factors	*International Tables for Crystallography* (1992, Vol. C)
Anomalous scattering factors	Cromer–Liberman

tions, 328 free parameters). The solution thus obtained was used as a starting point for the three-dimensional structure refinement.

2.5. Three-dimensional structure and 8 Å superstructure

The puzzle we had to solve to refine the three-dimensional structure was the problem of the atomic z displacements. Indications of atoms displaced from the atomic planes were obtained from Fourier difference maps. Furthermore, without introducing z displacements, wR remained too high.

As the atomic layers are mirror planes, each z displacement means introducing a split position with two atoms having opposite displacements. Furthermore, in many cases it appeared necessary for a triply split position, with one atom on the layer and two oppositely displaced. This result is rather cumbersome. Therefore, we introduced a z-displacement-based 8 Å superstructure,[5] compatible with the previously mentioned diffuse scattering interlayers. The model consists of

one flat layer (F^+) at $z = 1/4$, described by AS's **A**, **B**;

one puckered layer ($P^\uparrow$) at $z = 3/4$, described by AS's **A**′, **B**′;

one flat layer (F^-) at $z = 5/4$, described by AS's **A**, **B**;

one puckered layer ($P^\downarrow$) at $z = 7/4$, described by AS's **A**′, **B**′.

More specifically, layers $P^\uparrow$ and $P^\downarrow$ were constrained to be equal, except for the z displacement having opposite signs (positive and negative, respectively). Layers F^+ and F^- are flat and unconstrained. In particular, occupancy values in F^+ were restrained to be larger or equal to the respective values in F^-. These attributions are of course only conventional, because without reflections with semi-integer h_5 the F^+, F^- and the $P^\uparrow$, $P^\downarrow$ layer pairs appear overlapped. Many significant differences between two layers constituting an overlapping pair could be resolved due to different ADPs, but their assignment is arbitrary.

There are two plausible reasons for this ordering. Firstly, a locally high atom density in the F^+ layer might repel atoms of the adjacent puckered layers, so that they come closer to the layer F^-, which is less dense. Secondly, Co atoms in the F^- (or F^+) layer might attract Al atoms from the adjacent ones. The

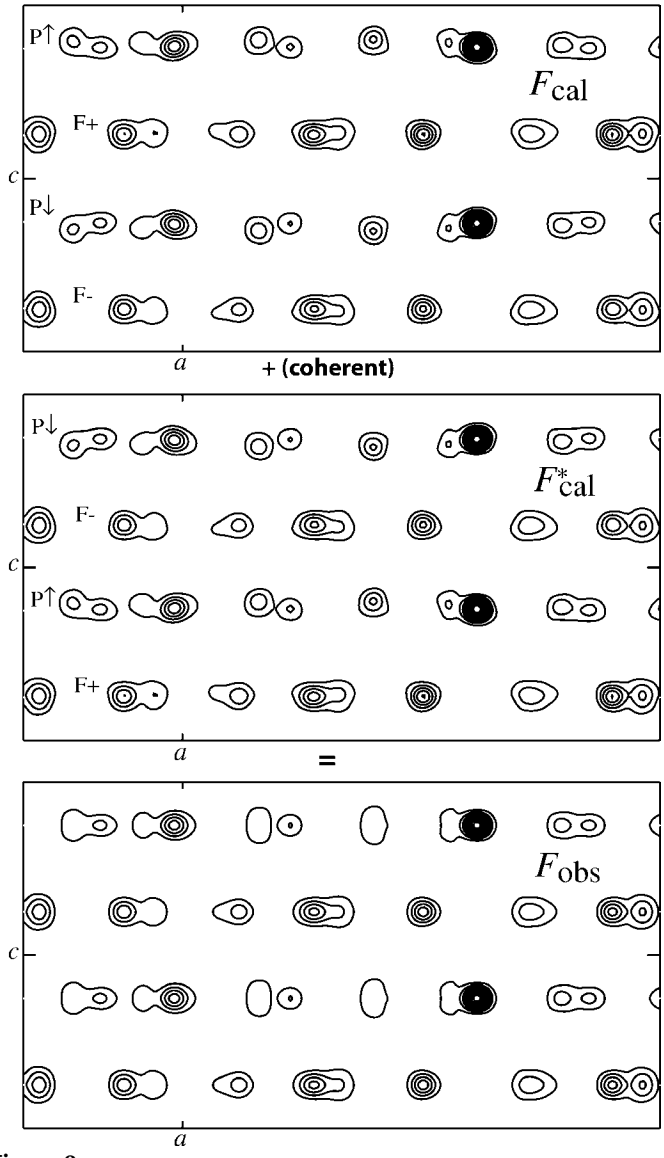

Figure 8
An illustration of the 8 Å superstructure, made by bounded projection along x_2 of the electron density in a parallelepiped (see Fig. 7*d*, yellow band). *Top*: the electron density of the structure in one type of domain. Calculated including unobserved reflections on the half-layers. *Centre*: the same after a shift of c along x_3, as it would be in the second type of domain. *Bottom*: F^{obs} plot, only observed reflections. It is clear how it can result from a coherent superposition of the former two maps. The reflections on the half-layers would be cancelled by destructive interference if we assume the same volume fraction for the two types of domains.

[5] The notation will be kept consistent with the 4 Å average structure throughout.

Table 3
Refined occupancies and areas of the Al and TM subregions of AS **A** in the F^-, the P ($\uparrow$ and $\downarrow$) and the F^+ layers.

	TM				Al			
	Occupancy			Area	Occupancy			Area
	F^-	P	F^+	[10^3a^2]	F^-	P	F^+	[10^3a^2]
1	1.000	1.000	1.000	5.860	–	0.100	0.452	4.109
2	–	1.000	–	2.620	0.152	–	0.502	4.240
3	–	0.405	0.407	4.109	0.295	0.296	0.495	4.240
4	1.000	1.000	–	1.620	0.202	0.350	0.252	4.497
5	0.700	0.701	0.500	4.240	0.345	0.450	0.295	2.620
6	0.656	0.755	0.906	4.497	–	0.846	–	2.620
7	0.649	0.503	0.699	2.620	0.902	–	0.952	4.240
8	0.205	0.149	0.355	2.620	1.000	0.101	1.000	2.620
9	1.000	1.000	1.000	1.620	1.000	1.000	1.000	1.001
10	0.454	1.000	0.705	2.620	1.000	1.000	1.000	0.619
11	1.000	–	1.000	2.620	0.901	0.252	0.801	2.620
12	0.357	0.705	0.707	4.240	1.000	1.000	1.000	2.620
13	0.155	–	0.555	2.620	–	0.751	–	4.240
14	0.257	0.210	0.207	4.240	–	0.750	–	1.001
15	–	0.202	–	1.620	0.401	0.550	0.501	1.620
16					–	0.550	–	2.620
17					0.452	0.550	0.652	4.240
18					0.601	0.751	0.401	2.620
19					1.000	0.051	1.000	2.620
20					1.000	0.700	0.752	4.240
21					1.000	–	1.000	2.620
22					0.352	0.900	1.000	4.240
23					–	1.000	–	1.001
24					1.000	–	1.000	1.620
25					0.452	0.301	0.452	4.240
26					–	0.150	–	2.620
27					0.900	1.000	1.000	0.619
28					1.000	1.000	1.000	1.001
29					0.451	0.201	–	2.620
30					0.801	1.000	1.000	2.620
31					0.702	1.000	0.602	4.240
32					0.101	0.150	0.301	1.620
33					–	0.550	–	2.620
34					0.951	0.452	1.000	2.620
35					0.301	–	0.151	2.620
36					–	0.600	–	2.620
37					0.802	–	0.802	4.240
38					–	0.550	–	4.240

latter is a much weaker variant of the 8 Å ordering in the (Co-based) PM phases.

This superordering should produce weak Bragg peaks on the semi-integer diffuse layers; to avoid that, we can imagine, as currently hypothesized by Steurer & Frey (1998) and Frey *et al.* (2000), a structure of columnar domains, having infinite extensions parallel to the periodic axis. The domains would be coherent in the projection onto the quasiperiodic plane (x_1, x_2), while some of them would be randomly displaced of length c along x_3 or of one unit along z.[6] This is illustrated in §2.7. With a volume partition near 50%, this would extinguish all Bragg reflections in the semi-integer diffuse layers. The diffuse part would remain, as it depends on the effective atomic distribution throughout all the partially occupied sites (Welberry, 1985), which is independent of the domain structure. As possible domain boundaries, all lines of zero vertical displacement in the $P^{\uparrow\downarrow}$ layers are of course plausible. In §2.7 we show that such lines coincide frequently with quasiperiodic tiling edges (of a PPT[1]), which agrees with the coherence hypothesis. The interface energy between different domains should be very low, because only a few cross-layer bonds might be affected. These considerations justify the equal volume fraction.

One more conceptual problem is the space group. The Laue group of this model remains $10/m$, but the corresponding superstructure space group is only $\overline{10}$, losing the 10_5 screw and consequently the observed extinction rule $(0000\,2n+1)$. However, this can be recovered as the effect of a strong pseudosymmetry. We decided to introduce a pseudosymmetry restraint, simply by adding to the data set seven fictitious reflections $\mathbf{h} = (0000h_5)$, with h_5 = 1,3,5,...13, with $F_\mathbf{h} = 0$ and assigning them high weights, empirically chosen as $100\max(w_\mathbf{h})$. This proved to be effective; the calculated F's remained well below the observability threshold, which is $\sim 10^{-4}\max(F_\mathbf{h})$. No easy explanation can be given for this pseudo-extinction.

2.6. Refinement method and results

We developed a capable software for the structural refinement of d-QC's. The main features are described in Haibach *et al.* (2000). The program minimizes a target function, which can be chosen between all those which are usually employed in crystallography. In the present case the target function has been chosen as

$$f = \sum_\mathbf{h} \left(\left|F_\mathbf{h}^\mathrm{obs}\right| - \left|F_\mathbf{h}^\mathrm{cal}\right|\right)^2 w_\mathbf{h},$$

where $F_\mathbf{h}^\mathrm{cal}$ is evaluated as the FT of the five-dimensional periodic structure model and $w_\mathbf{h} = 1/\sigma^2_{F_\mathbf{h}}$. The geometry of the AS's and their subdivision is given as input and not refined. Each subdomain has a specified chemical identity; mixed-chemistry regions are treated as separate congruent subdomains. For each subdomain in the asymmetric unit the refinable parameters are occupancy, anisotropic thermal factor (dynamic ADP's), physical space shift from the ideal cut-and-project position (static ADP's), anisotropic phasonic thermal factor and anomalous scattering components. The input card contains the geometric information together with the initial values of the refinable parameters. The actual refined parameters in each run are specified (each with its upper and lower bounds) in the second part of the input card, the remaining ones are fixed. The chosen refined parameters set can be subjected to a set of linear equality constraints and inequality restraints (specified in the third part of the input card). In particular, fractional composition of a given element and mass density can be constrained to a given value or restrained in an interval. Occupancies of subdomain pairs which happen to generate too-close atom pairs in physical space are also restrained so that their sum is less than one. For instance, mixed-chemistry regions generate overlapping atom pairs, so they need to be restrained. For more complex groups of short bonds one may give occupancy–sum restraints with

[6] In other d-QC's, columnar domains with $c/2$ displacements have been detected (Saitoh, Tsuda *et al.*, 1999); these domains need to be incoherent, unless all the reflections with odd h_5 be (pseudo)extinct. However, no indications of such nanostructure exist in basic d-Al–Co–Ni.

more terms or simply more two-term restraints. The short-bond conditions are to be determined separately at the beginning, then the resulting restraint equations have to be included in the input card. This geometric exercise (see Haibach *et al.*, 2000) needs some bookkeeping. It has also to be verified at successive stages of the refinement in the presence of high static ADPs.

In the presence of a very complex structure, it is necessary to use several cycles of partial refinement in which only a subset of the free parameters is used, before running on the full parameter set, which meanwhile can be reduced. The necessary first stage is to obtain a good initial estimate of all occupational and positional parameters (static ADPs): this can be performed in a higher-symmetry space group or, as we did, working in the z projection.

Constraints are also useful to reduce the number of free parameters. Some constraints (*e.g.* the stoichiometry, as we have a very precise estimate) can be simply kept fixed. For others (*e.g.* the density, whose value we could only infer) it is necessary firstly to test different values in a plausible range and then choose the one giving the best results; secondly, it is necessary, in the last stages, to refine it (removing the constraint) and check that the solution is stable. Many additional constraints can be derived from the restraint equations when these stabilize on the upper or lower bound.

The refinement results are given in Table 2. The observations-to-parameters ratio (3.7, for 749 parameters and 2767 observations) is high, but acceptable. However, by the careful procedure outlined above, convergence was achieved successfully. With regard to the short-bond occupancy–sum restraints, we noted that the summed occupancies rarely go to the bounds and even then mostly in a trivial way – with one of the occupancies to 1 and the other(s) to zero. In fact, only in the first part of the refinement are the short-bond restraints active.

To keep the refinement meaningful, on the last cycles we fixed to zero all the AS subregions with occupancy stable under 0.05, while those with occupancy above 0.99 have been fixed to 1. Neighbouring subregions have been merged when they are not particularly different in any respect. Static ADPs for the same subregions in different layers have been constrained to equality in the first phase. Successive tests revealed this situation to be stable, therefore, these constraints have been kept. A more detailed statistical analysis is shown by the logarithmic $F^{\rm obs}$–$F^{\rm calc}$ plot (Fig. 5*a*) and the detailed R-values distribution and F–σ_F analysis (Fig. 5*b*). In Table 2 we also report the values relevant to the subset of most reliable reflections (those with $I_{\mathbf{h}} > 3\sigma_{I_{\mathbf{h}}}$) and to the subset of reflections which would be ideally observable on a rotating-anode diffractometer, selected by a very liberal criterion $I_{\mathbf{h}} > 10^{-4}\max(I_{\mathbf{h}})$. Tables 3 and 4 report the refined occupancy parameters for all the surviving subregions of the atomic surfaces **A**, **B**, respectively. All other refined parameters, as well as the coordinates of the vertices of the AS's partition in subdomains, are deposited.

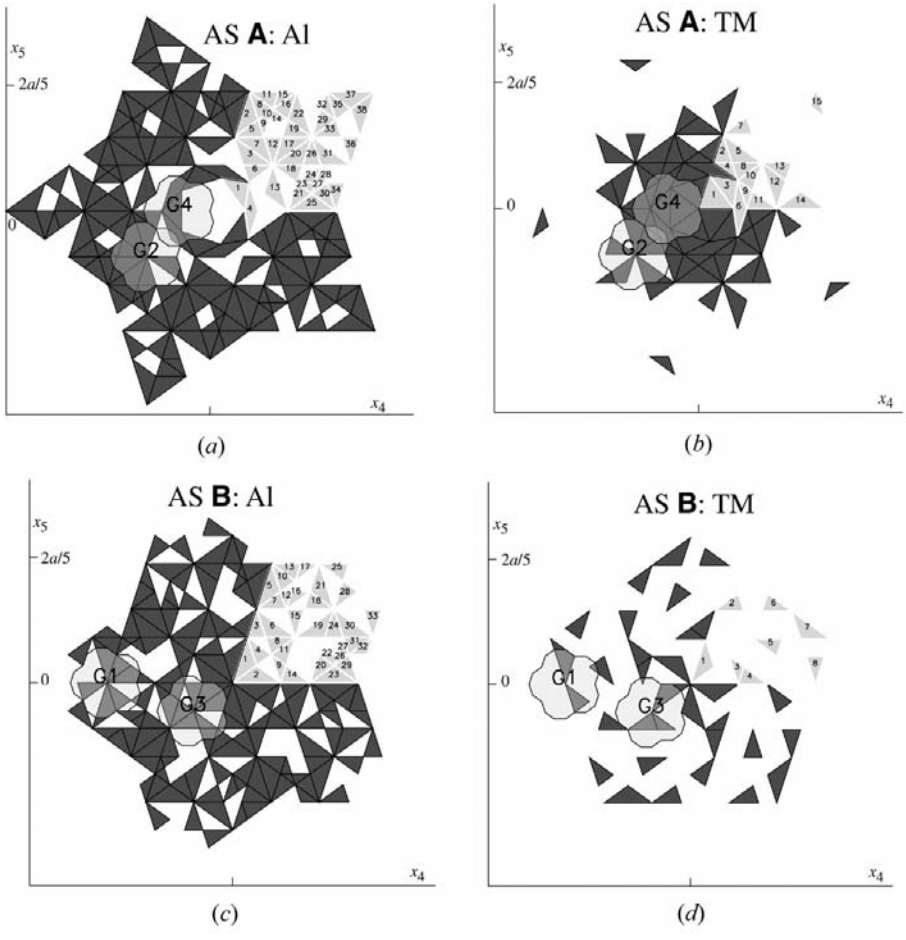

Figure 9
(*a*) AS **A**, Al subregions. Numbered, pale grey, the subregions in one asymmetric unit. The overlaid polygons marked with G4 and G2 are copies of the AS of Fig. 2, centred in the origin of the unit cell. This AS is the *locus* of the centres of 20 Å Gummelt decagons. The overlapping portions of AS **A** correspond to atoms located at a fixed physical space distance from the centre of one Gummelt decagon. This distance is a_r = 2.43 Å for G4 and $\tau^2 a_r$ = 6.37 Å for G2. Note how different clusters would have different decoration in the respective circles. (*b*) AS **A**, TM subregions. Same description. (*c*) AS **B**, Al subregions. Same description. Polygons G1 and G3 correspond to distances of $\tau^{-1}a_r$ = 1.50 Å and τa_r = 3.94 Å, respectively. (*d*) AS **B**, TM subregions. Same description.

2.6.1. Global parameters. Extinction is important in highly symmetric perfect intermetallic crystals. We evaluated different approaches to evaluate this effect, opting for a simplified version of the Becker–Coppens algorithm (multiple scat-

Table 4
Refined occupancies and areas of the Al and TM subregions of AS **B** in the F^-, the P ($\uparrow$ and $\downarrow$) and the F^+ layers.

	TM				Al			
	Occupancy			Area	Occupancy			Area
	F^-	P	F^+	$[10^3a^2]$	F^-	P	F^+	$[10^3a^2]$
1	0.500	0.653	0.450	4.240	0.495	0.100	0.545	4.240
2	1.000	0.549	1.000	2.620	0.702	0.300	1.000	4.240
3	1.000	0.648	1.000	1.620	0.901	0.100	0.901	2.620
4	0.598	0.603	0.598	2.620	1.000	0.550	1.000	2.620
5	1.000	0.903	1.000	2.620	0.152	0.102	0.052	4.240
6	0.354	–	0.354	2.620	0.802	1.000	0.852	4.240
7	–	0.205	0.107	4.240	–	0.446	–	2.620
8	0.504	0.703	0.554	2.620	1.000	1.000	1.000	2.620
9					–	0.346	–	1.620
10					0.201	0.450	–	2.620
11					1.000	0.800	1.000	2.620
12					0.401	0.350	0.401	1.001
13					–	0.150	–	2.620
14					0.396	0.150	0.396	2.620
15					–	1.000	–	2.620
16					0.851	1.000	0.951	1.620
17					0.501	0.850	0.501	1.620
18					0.501	1.000	0.601	2.620
19					–	0.400	–	4.240
20					1.000	0.400	1.000	2.620
21					0.052	0.900	–	4.240
22					0.051	1.000	0.251	1.001
23					1.000	0.850	1.000	4.240
24					–	1.000	0.451	2.620
25					0.251	0.150	0.451	2.620
26					1.000	–	1.000	0.619
27					0.601	1.000	0.601	1.001
28					0.051	1.000	0.101	2.620
29					0.051	–	0.151	2.620
30					–	0.400	–	4.240
31					–	0.150	0.151	2.620
32					0.901	1.000	0.951	1.620
33					0.151	1.000	0.351	2.620

tering in a single mosaic block; Becker & Coppens, 1974*a*,*b*, 1975; Thornley & Nelmes, 1974; Thornley, 1983). Extinction was evaluated as

$$\varepsilon_{\mathbf{h}} = \left[1 - \epsilon\left(F_{\mathbf{h}}^{\rm obs}\right)^2 \frac{1+\cos^4(\theta_{\mathbf{h}})}{1+\cos^2(\theta_{\mathbf{h}})}\right]^{1/2},$$

with $\theta_{\mathbf{h}}$ denoting the diffraction angle and ϵ the unique extinction parameter (its final value is reported in Table 2). The largest effect regards the reflection (00002), with $\varepsilon_{(00002)} = 0.62$.

The perpendicular space random displacement parameter $B^{\perp}$ (phasonic thermal factor, see §A2.2) was refined as an overall isotropic parameter; the significance of more detailed forms was estimated to be small. Its value of 0.51 (5) Å^2, corresponding to an r.m.s. displacement of $\left(\langle u_{\perp}^2\rangle\right)^{1/2} = 0.03a_r$ (the AS radius is $\approx a_r$), indicates a good structural regularity. The actual value might be smaller because this parameter may incorporate the effect of approximations implicit in the structure model.

The resulting value of the crystal density $D_x = 3.887$ Mg m^{-3} is in good agreement with literature values (3.94 Mg m^{-3}, see Table 1) for basic *d*-Al–Co–Ni of close composition. The corresponding point density is 0.06443 at. Å^{-3} (atomic volume 15.52 Å^3). Note that the density D_x is 7% lower than the measured value for *d*-Al–Co–Ni with ~13 at.% Co (Edagawa superstructure). The Edagawa phase is richer in Co and thermodynamically stable at lower temperature (1023 K) than the basic Ni-rich phase. These features are sufficient to explain the difference. If we take a Gummelt decagon (10.3 Å radius) as the volume unit, our refined density yields on average 41.25 atoms per decagon per layer; for the Edagawa phase, we would have only 3.1 more atoms per decagon per layer. Additional atoms would reduce the free space and the disorder degrees of freedom, as expected. Longer-range local correlations in a denser phase would also explain superstructure ordering. A more complete answer will be given by a detailed structure solution of the Edagawa phase, which we plan to undertake.

A note is necessary on the reliability of the measured mass density values. Due to the frequent observation of micro-voids in QCs, it has been argued that measured density values might be severely biased. A simple calculation, assuming equal spherical voids arranged on an f.c.c. (face-centred cubic) lattice, shows that, to obtain a 7% void volume fraction, the minimal centre-to-centre separation must be exactly 2.2 times the void diameter. For a more reasonable five-diameter separation we have only 0.56%. The only measured value we found for the void volume fraction in QC's (Mancini *et al.*, 1998) is 0.2%. Typically, an experimental error of 1% on the density is found and the bias due to micro-voids can be neglected.

2.7. The refined structure: graphical presentation

Conventional representations of a quasiperiodic, strongly disordered structure are not possible or meaningful. Therefore, we have to illustrate this structure in original ways, selecting the most informative views.

Fig. 6(*a*) shows the projected structure at a resolution reduced to 1 Å, with overlaid (contours) full-resolution map. A decagonal 'flower' composed of five partly overlapped Gummelt decagons is also overlaid. This plot shows roughly how the structure might be seen at the typical resolution of an electron microscope. The decoration of the Gummelt decagons appears simplified and the differences between decagons are less visible, although they were already noted by Yan *et al.* (1998). This has led to a proliferation of simplified structure models, based on different interpretations of low-resolution HRTEM or HAADF images, see §3.2. The asymmetry of the decagons is also clearly visible, in agreement with most observations. Fig. 6(*b*) shows the projected structure electron density, drawn by contour levels. The resolution, evaluated as $0.25\lambda/\sin(\theta_{\rm max})$, is 0.15 Å. Several structure motifs discussed in the text are overlaid. Fig. 6(*c*) shows the projected TM contribution to the electron density. Colour-coded: contributions from the averaged F^+, F^- and $P^{\uparrow}$, $P^{\downarrow}$ layers. Some atom pairs, corresponding to interlayer bonds < 3 Å, are evidenced by rectangles. These should be nickel sites, as shown by polarized EXAFS on *d*-Al–Co–Ni (Zaharko *et al.*, 2001): Co atoms do not have TM neighbours under 3 Å, while Ni atoms

do. The latter form zigzag chains along the periodic axis, as hypothesized by Cockayne & Widom (1998*b*). In contrast, some isolated TM sites may be attributed to Co. TM assignment cannot be carried out for all sites, because partial occupation frequently causes indecision.

In Fig. 7 the $F^{\rm calc}$ electron density is represented in detail. The $F^{\rm diff}$ electron density, not shown, is very low (maximum voxel value 2.4% of the maximum $F^{\rm obs}$ voxel in a $12a \times 12a \times 2c$ volume grid of $1200 \times 1200 \times 200$ points) and featureless. In particular, Figs. 7(*a*) and (*b*) show the electron density for the two F^{+}, $P^{\uparrow\downarrow}$ layers, respectively. Separate contributions from Al and TM are evidenced in different colours. The contour levels for the Al contribution are scaled by $Z_{\rm Al}/Z_{\rm Ni} = 13/28$. The layer F^{-} (not shown) is structurally similar to F^{+}. Fig. 7(*c*) shows the x_3 moment of the electron density on the $P^{\uparrow\downarrow}$ layers, to evidence which atoms are most displaced from the layer plane. The layer x_3 moment is defined as

$$\int_{-\infty}^{+\infty} {\rm d}x_3\,(x_3 - x_3^L)\,\rho_e^L(x_1, x_2, x_3, 0, 0),$$

where x_3^L is the ideal coordinate of the layer plane and ρ_e^L the electron density of all and only the atoms in the layer considered to be single. Note that most tile boundaries of a PPT[1] (green lines) are zero-moment lines, therefore, they are possible domain boundaries. Also to be noted is the weak breaking of the mirror symmetry (mirror plane orthogonal to x_2). It is clarified that the effect is due to small occupancy differences in several sites rather than large differences in a few sites.

Fig. 8 is a parallelepiped-bounded projection along x_2, useful to illustrate our concept of the 8 Å superstructure in terms of coherent domains.

Figs. 9(*a*)–(*d*) represent the partition of the AS's **A**, **B**, with separate representations for Al and TM (this is necessary due to their large overlap). Their complex shape stimulates reflections on the AS's nature. We determined them as the union of polygonal-shaped subdomains. Another group (Elcoro *et al.*, 1994) put forward the use of symmetry-adapted functions to describe the AS's boundaries. They have obtained encouraging results (Elcoro *et al.*, 1995) with simple models (see §3.1). From the computational point of view, the advantages of this approach (slight reduction of free parameters) probably do not compensate for the more complex calculation of the Fourier transform. The use of symmetry-adapted functions is interesting in a broader sense, that is to model the probability density on the AS's, using continuous smooth functions rather than piecewise-constant ones. Furthermore, as we observe significant static ADP's, the shape of the AS's might be better described as two-dimensional varieties rather than (piecewise) flat polytopes parallel to $E^{\perp}$. Presently, the use of symmetry-adapted functions to describe both four-dimensional shape and occupancy of the AS's seems appealing, even if theoretically arduous.

It is customary to present, as a further assessment of the quality of the structure solution, $F^{\rm obs}$–$F^{\rm calc}$–$F^{\rm dif}$ Fourier maps of the AS (*i.e.* x_4x_5 sections passing through the AS centres and on the x_1x_4 section, which contains the four-dimensional cell body diagonal). We did calculate such maps, necessarily limited to the average 4 Å structure ($P\overline{1}0$). To compensate for the z-ADPs, we used bounded z-projections with thickness $\pm c/4$ around the average atomic layer. These maps were not very informative. The AS structure is better represented in Fig. 9. The $F^{\rm obs}$–$F^{\rm calc}$ maps are not sensibly different. The $F^{\rm dif}$ maps appear very weak and featureless. Taking as a 100% level the centre of AS **A** (maximum for all sections), the maximum difference appears in the AS **B** and AS **B**′ x_4x_5 sections, amounting to less than 2%. The plots are included in the supplementary material.

2.8. Local (dis)order: comparison with approximant PM phases

It is very difficult to make any meaningful autonomous structural discussion. Given the statistical nature of most atomic sites, this would take a lengthy and cumbersome listing of probable local configurations. However, some regularity can be noticed. Atomic motifs compare well with those occurring in approximant PM phases and in PM-approximant-based structure models of *d*-QC's (Saitoh, Tsuda *et al.*, 1999; Yan & Pennycook, 2001; Cockayne & Widom, 1998*a*).

Consider the tiles of the PPT[1], drawn as green lines in Figs. 6(*b*), and 7(*a*) and (*b*). First, divide them into 'acute' and 'obtuse' tiles (the former having at least one vertex angle of $\pi/5$). The acute tiles are decorated by linear atomic motifs, along the bisectrix line of the $\pi/5$ angle(s). The obtuse tiles are pentagons (3.94 Å radius) which appear in two orientations, say 'right' and 'left', respectively, if they have one vertex to the right or to the left of the centre. In projection (Fig. 6*b*) the decoration of both is similar, roughly a centred decagon of radius a_r. This decagon decomposes in two inverted pentagons on two neighbouring layers (Figs. 7*a* and *b*). A pentagonal-biprismatic column results (as in Steurer *et al.*, 1993), also common in PM phases (Grin *et al.*, 1994*b*). In the flat layers, 'right' pentagons of the PPT[1] contain one *centred* a_r pentagon of atoms; the centre often has mixed chemistry, while the pentagon can often be decomposed in a TM acute triangle (some evidence given in Figs. 7*a* and *b*) plus two Al atoms. From the low values of site occupancy, approximately two TM atoms and one Al atom may be distributed on these sites. Always in the flat layers, the 'left' PPT[1] pentagons are decorated by non-centred atomic pentagons; these have mixed chemistry, low occupancy and the result is often deformed (squashed). In the puckered layers, we repeat the same considerations, just inverting the roles of 'left' and 'right' PPT[1] pentagons. About the z displacements, from Fig. 7(*c*) it is evident that in the centred a_r pentagons often only the central atom is displaced, while in the uncentred ones all the five pentagonal sites are displaced. Other important a_r antiprismatic pentagonal columns are formed at the junction of three PPT[1] pentagons, in the centre of GDC[3] (see Figs. 7*a* and *b*).

The most important motif present in (Al–Co) approximant PM phases is the pentagonal bipyramid, or PBP, of Cockayne

& Widom (1998*a*; *cf.* Fig. 2 of that work). This motif is structured on four layers (8 Å). The basal layer (A) contains a flat TM pentagon, with the size of the PPT[1] pentagons (4 Å radius). Al atoms are found in its centre and intercalated on the edges. Below and above (B layers), there are two pentagonal caps, that is, TM-centred a_r pentagons of Al; these belong to puckered layers, because the central TM is pushed away from the central Al of layer A. There is a fourth layer (C) as a junction, with another TM-PPT[1] pentagon and five Al atoms forming a squashed a_r pentagon inside; the centre is free. The alternance is then BABC.... In our structure this complex configuration is not found as such, but a modified version with layer A replaced by another C layer (quasi-PBP). We have sequences BCBC..., either with the B's on the F^+, F^- layers and the C's on $P^\uparrow$, $P^\downarrow$ layers or *vice versa*. This is evidenced in Figs. 7(*a*) and (*b*). The TM-centred a_r pentagons of layers B are formed by Al and TM and not only Al; in correspondence, their TM vertices are shared with the TM-PPT[1] pentagon of a neighbouring quasi-PBP. Many sites are statistically occupied. A strong *z* displacement of the TM centre of B is no longer necessary; rather, the inner Al atoms of C are often displaced.

The chemical reason for the differentiation of the quasi-PBP is most certainly the substitution of most Co by Ni. This is, on the atomic scale, the reason for the loss of a larger differentiation on the 8 Å four-layer sequence, discussed in §1.3.5.

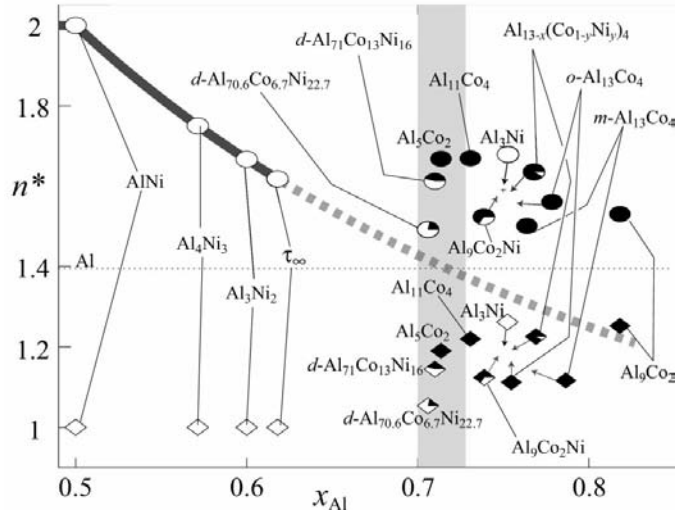

Figure 10
Numeric atomic density n^* *versus* Al fraction x_{Al} representation for all the known Al-rich Al–Co–Ni phases. *Circles*, the total numeric atomic density; *rhombs*, the partial numeric atomic density of Al atoms. n^* is in units of atoms per β -AlNi b.c.c. (body-centred cubic) cell (lattice parameter 2.88 Å). The Co:Ni partition is represented by black:white angular sectors in the symbols. The dotted thin line is the n^* value for natural (f.c.c.) Al. The thick grey curve represents the behaviour of the VOPAS phases (all Al–Ni binary); the continuous part represents a continuum of off-stoichiometric Al_xNi_{1-x} (x = 0.5,... 0.62) experimentally determined phases, while the dashed part is an ideal continuation. The grey vertical band is the stability region of *d*-Al–Co–Ni. Note that the two *d*-QC's represented here are a junction between the VOPAS AlNi phases and the (mostly Co-based) PM phases, clustered on the right.

Important indications originate from statistical mechanics simulations (Cockayne & Widom, 1998*b*; Krajčí *et al.*, 2000; Mihalkovič *et al.*, 2001). Simulations based on local pair interactions can reproduce well the local atomic structure of known PM approximants. On the other hand, the quasiperiodic long-range order is not reproduced at all. HBS-type (hexagon–boat–star) random tilings form instead. This indicates that the key interactions responsible for the long-range order must be of non-local nature (see §2.9), while local configurations are determined mainly by local interactions, independently from periodicity or quasiperiodicity.

2.9. Global order: comparison with VOPAS phases

2.9.1. QC–VOPAS structural comparison. The study of the structural relation of QCs with VOPAS phases is much less popular with respect to the PM phases, because the local order (atomic motifs) is very different. Few works (Chattopadhyay *et al.*, 1987; Dong, 1989; Dong *et al.*, 1994; Mandal & Lele, 2000; Zhang *et al.*, 2000; Steurer & Cervellino, 2001) put forth this topic. However, this relationship is not less important; QC is possibly a convergence point, or better, a fortunate combination of the pentagonal local order of PM phases with the long-range ideal order of VOPAS phases. The ternary composition of most stable QCs fits well in this frame. Consider the Al-rich part of the Al–Co–Ni phase diagram. All but one of the Al–Co (pseudo)binary phases (listed in §1.1.1 and Fig. 10) are characterized by pentagonal motifs; the exception is Al_9Co_2 (Douglas, 1950), the only one with >80 at.% Al. This is completely different for Al–Ni phases. Here, only one phase (Al_3Ni; Bradley & Taylor, 1937*b*) shows pentagonal structure motifs, see Steurer (2001*a*) and references therein. All other Al–Ni phases (see §1.1.1 and Fig. 10) can be described as vacancy-ordered CsCl-type (β-type, B2-type) derivative structures. Why do Al–Ni phases show vacancy-ordering but Al-Co phases do not? The defect energetics of the Al(Ni,Co) β phases have been thoroughly studied (Alavi *et al.*, 1999; Bester *et al.*, 1999; Korzhavyi *et al.*, 1999; Börnsen *et al.*, 2000; Schapink, 2001), clearly showing in the case of Ni a higher energy for Al_{TM} substitutions than for TM vacancies. On the other side, this energy difference in the case of Co is marginal.

Vacancies play a structural role also in QCs. Several positron-annihilation studies on *d*-Al–Co–Ni (Nakao *et al.*, 1992), as well as on other Al-based QCs and on related PM-approximant phases (Ohata *et al.*, 1990; Nakao *et al.*, 1993; Lawther & Dunlap, 1994; Kanazawa *et al.*, 1994; Würschum *et al.*, 1994, 1995; Kanazawa *et al.*, 1997; Sato *et al.*, 1999), have been performed. They all indicate a very high concentration of structural vacancies in QCs and a much lower concentration in PM phases. Furthermore, as the density of vacancies seems to increase with the perfectioning of quasiperiodic order during annealing (Prekul *et al.*, 1998), they are not to be thought of as mere defects.

The notion of PAS of a *d*-QC is a concept mutuated from the world of incommensurately modulated structure (IMS, see Steurer & Haibach, 2001), to which many QC's can be reduced. The PAS we deal with is amenable to the CsCl-type AlNi structure (Steurer, 1999*a*); in a centred orthorhombic setting its primitive vectors are parallel to the x_1, x_2, x_3 axes. Details are recalled in §A3. With our refined numeric density, a PAS unit cell contains 1.492 atoms (cubic setting) or 2.984 atoms (orthorhombic setting). The QC's electron density (or the atomic positions) can be averaged in the PAS unit cell; alternatively, the QC's atomic site position vectors can be reduced into one unit cell modulo lattice translation. The results can be interpreted as an (electronic or atomic) probability density (PD) in the PAS unit cell. This PD results from the quasiperiodic modulation. If the PAS has effectively a strong structural relationship with the QC, the PD should keep resemblance with a CsCl structure, with relatively narrow PD peaks rather than atoms. In terms of five-dimensional embedding, the PD peaks are just the obliquely projected AS pairs of each layer (Steurer & Haibach, 1999*b*; Steurer, 1999*a*, 2000). In Fig. 11 the electronic and atomic PD in the PAS cell are represented. For the layer F^+, Figs. 11(*a*), (*c*) and (*e*) show the total electron PD, the atomic PD for TM and the same for Al, respectively. Analogue representation is given in Figs. 11(*b*), (*d*) and (*f*) for the layer $P^\uparrow$. To plot the atomic PD, the coordinates of millions of atomic sites in a 500*a*-radius circle were calculated by the cut method from the refined AS. The ungainly shapes result from the oblique projection and from the action of the (x_1, x_2) refined relaxation shifts for every AS subregion. However, the fundamental point is that the structural relationship is effectively strong. The effect of partial site occupancy is to smooth the contours of the PD. Also relaxation shifts have their importance (see the TM plots) as they smooth the PD towards the outside of each AS pair. As a result, the scattered intensity on the PAS reciprocal lattice Λ^*_{AV} will decrease rapidly at large $|\mathbf{q}|^{\|}$. Λ^*_{AV} in the IMS perspective is the lattice of the main reflections. In fact, it is a rarefied subset of the QC's reciprocal lattice, but it collects a significant fraction (17%) of the total scattered intensity.

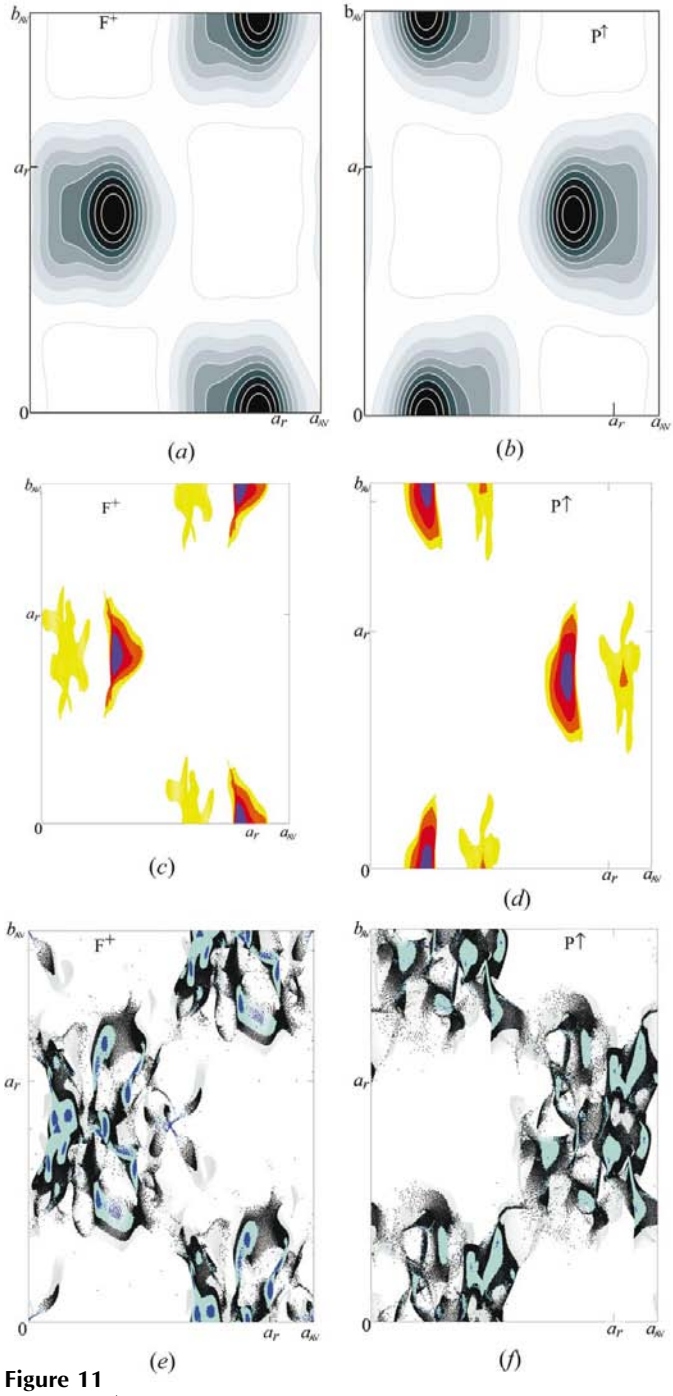

Figure 11
(*a*) Layer F^+: electron density of *d*-$Al_{70.6}Co_{6.7}Ni_{22.7}$ averaged in the PAS unit cell; (*b*) the same for layer $P^\uparrow$. (*c*) Layer F^+: average distribution of TM atoms in the PAS unit cell. The TM atomic sites calculated for *d*-$Al_{70.6}Co_{6.7}Ni_{22.7}$ on a 500*a* radius circle have been reported as modulo lattice translations in this unit cell. Site occupancy has been rounded off to values of 0.25 (yellow), 0.5 (orange), 0.75 (red) and 1 (violet); (*d*) the same for layer $P^\uparrow$. (*e*) Layer F^+: average distribution of Al atoms in the PAS unit cell. Site occupancy has been rounded off to values of 0.25 (pale grey), 0.5 (dark grey), 0.75 (azure) and 1 (blue); (*f*) the same for layer $P^\uparrow$.

2.9.2. QCs as a junction point?. The double structural relationship (QC–PM phases and QC–VOPAS phases) can be better understood in terms of the Hume–Rothery effect (see §4.2). The experimental determination of the pseudogap in the three types of phases (Belin-Ferré *et al.*, 2001) points clearly in this direction. We will try now to link the structural and physical comparative analysis. The parameter upon which the comparison is based is the *e*/*a* (valence–electrons per atom) ratio (Mayou, 1994; Dong *et al.*, 1994; Zhang *et al.*, 1997); however, the assignment of a valence number to TM is not univocal and also the position of strong Bragg reflections has to be considered. Ellner *et al.* (1989) instead use the Norbury criterion (in terms of Al electron density, e $Å^{-3}$). We chose a representation in terms of (total and partial for Al) numeric atomic density *versus* Al fraction, which is more universal and anyhow easily amenable to the former. In Fig. 10 this representation is given for all known phases in the Al-rich side of the Al–Co–Ni phase diagram. The reference volume is the β-AlNi unit-cell volume (a cube of 2.88 Å edge). It is evidenced in the trend followed by the β-phase-related VOPAS phases (all binary Al–Ni); symbols mark the stoichiometric point of each phase. Off-stoichiometric alloys have been determined to

Table 5
Comparison with the structure model of Takakura *et al.* (2001) (model T in the table).

Here set II is the full synchrotron data set of this paper, reduced in space group $P10_5/mmc$ (1544 unique reflections); set I is a subset of set II (451 reflections with the highest F/σ_F ratio, approximately corresponding to that used by Takakura *et al.* (2001). Model T has been considered 'as published' (only the scale factor and extinction refined) and after partial refinement (global parameters and all static and dynamic ADP's); refinement carried out based on either set I and II. All values are in %.

	All reflections		Restriction to $(h_1h_2h_3h_40)$	
	R	*wR*	*R*	*wR*
This work				
Set I	5.5	5.3	7.2	7.0
Set II	17.0	6.0	14.5	7.7
Model T: 'as published'				
Set I	12.2	12.5	10.0	10.5
Set II	30.1	25.3	28.7	24.5
Model T: after refinement based on set I				
Set I	8.8	9.1	10.2	12.9
Set II	34.9	30.3	37.5	38.8
Model T: after refinement based on set II				
Set I	8.8	9.1	10.2	12.9
Set II	24.6	19.6	25.7	23.8

follow the continuous line with continuity (Bradley & Taylor, 1937*a*; Ellner *et al.*, 1989). The dotted line extends ideally the VOPAS behaviour to the *d*-Al–Ni–Co stability region. Note that for many other Al-based QCs (with ∼60–65% Al) there is no need for an ideal extension, because the two regions are contiguous. The τ_∞ phase is a unidimensionally quasiperiodic, vacancy-ordered phase (Chattopadhyay *et al.*, 1987). Also represented are all the (generally Co-based) PM phases, which visibly form a separate group. The two *d*-Al–Ni–Co phases, the present one and the Edagawa phase (data from Chernikov *et al.*, 1998), are placed just between the two groups, behaving coherently with their Co content. This confirms the concept of *d*-QC's as the junction of PM and VOPAS phases.

3. Comparative model analysis

Our structure model for *d*-$Al_{70.6}Co_{6.7}Ni_{22.7}$ is the last of a long series which have been proposed in the course of a decade. Quite naturally, we need to make a comparative review of all the former models. We will proceed by (loosely) grouping the models in different categories, for the sake of clarity.

3.1. Early models

One of the first models proposed for *d*-Al–Co–Ni is due to Yamamoto *et al.* (1990). This model is not strictly comparable with ours; in fact, it is built for a QC of different composition (very Co-rich), different space group and different AS structure (mentioned in §1.3.5) than the one we deal with. Its experimental verification is insufficient (only 49 Bragg reflections have been considered). It would be interesting to verify this model on a robust data set for Co-rich *d*-Al–Co–Ni.

A passepartout model has been proposed for *d*-QC's in Burkov (1991), modified in Burkov (1993). The interesting point of these works is the introduction of the concept of covering, later developed rigorously by Gummelt (1996). The models in question are, however, fairly inadequate, with many incorrect basic assumptions. First, they introduce a 'universal' two-AS's configuration for *d*-QC's. As can be seen from §1.3.5, this is a very coarse approach. Then, the AS's construction in Burkov (1993) is based on the 'tiling decoration' method (see comment in §§2.2 and 3.2). The assumption of a universal 'magic composition' (Al:TM = τ:1 or $Al_{62}TM_{38}$) is clearly wrong. The model density is 20% too high, creating many impossibly short distances (2.2 Å). The TM ordering rule – the central point – has been disproven (Zeger *et al.*, 1999; Cockayne & Widom, 1998*b*). No meaningful experimental comparison is given in the original works. With our data, both models give $wR \simeq 0.5$ and $R \simeq 0.8$ ($I>3\sigma_I$). A substantially improved version, including statistical mechanics relaxations (Krajčí *et al.*, 2000; Mihalkovič *et al.*, 2001) has been compared with 253 Bragg reflections (data from Steurer *et al.*, 1993), resulting in a not exciting $wR = 0.14$.

Yamamoto (1996) proposed another model for *d*-Al–Co–(Cu,Ni), partly based on electron micrographs by Hiraga *et al.* (1994); see also §3.2. It is again a combination of an AS model with a tile decoration model. No experimental comparison except electron microscopy is given. With our data, $wR \simeq 0.5$ and $R \simeq 0.8$ ($I>3\sigma_I$). The tiling (pentagons plus decagons, adapted from Hiraga *et al.*, 1991, 1994) is peculiar, *cf.* the discussion of Kepler's *Aa* tiling in Lück (2000). With respect to the more known Gummelt decagonal cluster, the central part (decagon) is divided from the external part (ten pentagons) Fig. 6(*b*) shows this in detail. The decoration follows the symmetry of the corresponding polygons. The decagonal symmetry of the central part is particularly questionable; recent TEM observations (Abe, Saitoh *et al.*, 2000) deny it, others (Yan *et al.*, 1998) confirm it, but only for some clusters. We do not find a unique cluster; in some cases (see Fig. 6*a*) the central part appears more decagonal, in others less, but never exactly.

Another early model, proposed by some of us (Steurer *et al.*, 1993), has been elaborated on electron density maps obtained by maximum-entropy methods, based on only 253 unique Bragg reflections. The sample ($Al_{70}Co_{15}Ni_{15}$) was actually a superstructure (Steurer & Frey, 1993). Satellites had not been considered, so the average structure of this phase has been determined. This turns out to be quite similar to the basic phase, even if its measured density is larger by 7%. A small supplementary AS in $q = 0$ is the main qualitative difference. The electron density maps agree excellently with our present results, compare our Figs. 6 and 7 with Figs. 7 and 8 of Steurer *et al.* (1993). Difficulties in the electron density interpretation and the small number of independent observations (253) have led to a simplified AS-based structure model. Partial site occupancies in AS **B** (there named hyperatom 2) were not considered. With the original data, this simple model yielded a rewarding $wR = 0.078$. Our data set, with many more weak reflections, is much more selective and on the same model it yields $wR \simeq 0.35$ and $R \simeq 0.5$ ($I>3\sigma_I$). However, structural and crystal-chemical considerations are still – *mutatis mutandis* – valid. The proposed cluster (*monopteros*) is

compatible with the 20 Å diameter decagon widely discussed afterwards (see §3.2.2). Cluster overlap was not considered; however, careful inspection of Figs. 8 and 12 of Steurer *et al.* (1993) shows clearly that overlapping clusters are present. They were not recognized because of slight differences in the atomic decoration of different clusters, in agreement with the present work. An interesting variation of this model (Elcoro *et al.*, 1995) has been presented, which uses symmetry-adapted functions to describe the AS's (see §2.7).

3.2. Electron-microscopy-based models

3.2.1. General remark. The great limiting factor of electron microscopy (EM), when compared with XRD, is the lower resolution. Only recently, by employing new methods such as high-angle annular dark-field (HAADF) electron microscopy, the point resolution could be lowered to 1 Å; XRD still offers an improvement of an order of magnitude. Fig. 6(*a*) shows clearly the consequences. Complex patterns of partly occupied atomic sites are lost. The electron density is simplified; its peaks are irregular and the assignment of atoms to them is neither simple nor univocal. TM atoms are generally well visible, while the majority of Al sites (also scarcely populated) are not.[7] This is one reason for the proliferation of slightly different structure models for *d*-Al–Co–Ni. Furthermore, only the projected structure (usually on the quasiperiodic plane) can be seen by electron microscope. The separation of two screw-related atomic layers is possible, but the fine details of the three-dimensional structure and the 8 Å superstructure are invisible.

No EM-based analysis could address a structure solution as detailed as this study. Many contain excellent analyses. The error of simplifying the atomic structure as the decoration of one (or few) cluster or tile(s) is generalized. The cluster decoration plus the tiling rule are always presented. In the few cases in which the authors also give a five-dimensional representation we could make comparative refinement. The best result was the model from Saitoh *et al.* (1998), with $wR = 0.317$, $R = 0.372$ on 2287 reflections ($F > \sigma_F$). This is about the best result possible for a deterministic model (without partial site occupancy); the shape and composition of the AS's is about correct, even a small TM region in the centre of **B** has been determined. It is similar to our model in Cervellino *et al.* (2000), the best result we had with ideal QC models.

The simplicity of the electron density in low resolution is not only, however, a cause of trouble for EM analysis. It is significant for the interaction of electron waves with wavelength ~1 Å (typical for states near and below the Fermi level; Mayou, 1994; Dong *et al.*, 1994) with the crystal structure. This in turn is important to understand the stability of QCs and the mechanism of creation of long-range quasiperiodic order.

3.2.2. Model discussion. Many EM models are based on the composition $Al_{72}Co_8Ni_{20}$, very close to our sample and plausibly exactly the same structure (basic decagonal phase). Others regard a composition with 15 at.% Co, which is the Edagawa superstructure. On the level of accuracy of EM, the average structures likely coincide, so we will not stress the difference. Useful hints about the Edagawa superstructure ordering are given in Saitoh, Tsuda & Tanaka (1997), Hiraga *et al.* (2000) and Hiraga *et al.* (2001). The detailed structure solution of the Edagawa superstructure will be our next effort.

Hiraga *et al.* (1991) first identified the regular arrangement of 20 Å diameter decagonal columnar clusters which has been the basis of most subsequent analyses on *d*-Al–Co–Ni. The decagon cluster is decomposed in a smaller decagon surrounded by pentagons, to justify the cluster linkage. The clusters are linked by contact or by overlap of type A (see §A2.1). These rules (which correspond to the A and B overlap rules of Gummelt, 1996, applied to τ-inflated decagons) are the basis of several other works (Burkov, 1991, 1993; Yamamoto, 1996). The atomic decoration they proposed and that developed in Hiraga *et al.* (1994) was also considered by other authors (Burkov, 1991; Yamamoto *et al.*, 1990; Burkov, 1993; Yamamoto, 1996). The poor resolution available at the time (>2 Å) accounts for its gross inadequacies. Remarkable, however, in Hiraga *et al.* (1994) is the identification of a PPT[1] as the structure framework, agreeing with our correlation analysis (§1.3.3). An improved version of this model (Hiraga *et al.*, 2000, 2001) has been obtained with better techniques (1 Å resolution). The TM and Al arrangements are (within the EM limitations) mostly correct, except the cluster centre, where it is proposed an unreasonable alternance of pure Al and pure TM pentagons on the two layers. This would severely break the 10_5 (pseudo)symmetry and the observed $h_5 = 2n + 1$ extinction.

Tsuda *et al.* (1996) opened the discussion on the symmetry of the basic 20 Å diameter cluster. The cluster symmetry is proposed for the first time to be pentagonal rather than decagonal. The global arrangement of pentagonal clusters is proposed as the reason for the different space groups ($P10_5/m\,mc$, $P\overline{1}0m2$, we add $P10_5/m$) observed in different *d*-Al–Co–Ni phases. This line of thought was developed in Saitoh, Tsuda & Tanaka (1997) and Saitoh, Tsuda, Tanaka, Kaneko *et al.* (1997). Subsequent works (Steinhardt *et al.*, 1998; Abe, Saitoh *et al.*, 2000) reduced further the cluster symmetry to *m* (in connection with the overlap rules of Gummelt, 1996), while other works (Yan *et al.*, 1998; Yan & Pennycook, 1999, 2000, 2001) prefer to consider a decagonal cluster, whose decoration may happen to be locally different due to disorder. We confirm the low symmetry (1) of the 20 Å diameter cluster and also the existence of several slightly different variants. The cluster arrangement gives rise to the global (pseudo)space group $P10_5/m\,mc$, slightly broken into $P10_5/m$ (or better $P\overline{1}0$). The variant clusters are intrinsic in our AS's solution, disorder does not come into question. Let us imagine the decagonal cluster divided into rings, starting from the centre. The atomic decoration of each ring is decided by the overlap of the AS defining the cluster centres (CCAS hereafter; see §1.3.3) with the AS's **A**, **B**, **A**′, **B**′ which define the atomic structure. The overlap geometry depends on their

[7] In cited works sometimes simulation of EM images from the model therein are shown. They always appear much sharper than the real images, which compare generally better with our Fig. 6(*a*).

physical space distance; for each ring we must consider a distance equal to its radius r. For the first two rings (r = 1.5 and 2.4 Å) the CCAS centre falls on the points marked with G on **B**, **A**, respectively, for the two rings. We consider the two rings together because they constitute split positions only 0.9 Å apart; recall the squashed pentagons of Saitoh, Yokosawa *et al.* (1999). The G points, located at a_r/τ^2 (a_r/τ) from the AS **A** (**B**) centre, are important branching points of the AS's decoration. Depending on the position of each cluster centre in the CCAS, these rings will contain different mixtures of Al or TM, from AS **A** or **B**. The dogma of the unicity of the covering cluster (Steinhardt *et al.*, 1998; Abe, Saitoh *et al.*, 2000) has to be reconsidered. However, this feature is not necessary by any point of view; overlap rules and energetic considerations are well compatible with a finite number of slightly different clusters as well, which is a more general situation. Of course, the complication of building a multiple-cluster decoration model is enormous, surpassing greatly the AS's modelling method. The actual cluster arrangement, likely more complex than the Penrose tiling, has also to be determined case by case. The structural complexity of *d*-QC's requires a heavy tribute.

A remark about the large occupational/chemical disorder of our model and the possibility to investigate, by EM, its relation to the actual atomic structure is needed. By XRD we can only see the global three-dimensional statistical structure averaged on the coherent volume. For this QC, the unstructured nature of the diffuse scattering in the quasiperiodic planes indicates only short-range correlations therein (within the atomic bond length). In general, short-range order and thermal diffuse scattering can also explain curious diffraction features at the Bragg peak foot (Abe, Tamura *et al.*, 2000). The semi-integer diffuse layers are explained by our superstructure model. It is possible to hypothesize longer-range vertical[8] correlations inside each columnar cluster, giving rise to three-dimensional extended diffuse phenomena, too weak for XRD observation. On the other side, EM is a *local* probing technique, but it always averages the structure in the periodic direction on many atomic layers. EM could detect *local* cluster structures, stemming from intemediate-range vertical correlations, only on the limit in which the analyzed vertical thickness is smaller than the relevant correlation length. Vertically uncorrelated disorder would remain unresolved, unless single atomic layers could be probed.

A few words are also needed regarding the atomic decoration of the clusters. Models (Hiraga *et al.*, 1991, 1994; Tsuda *et al.*, 1996; Saitoh, Tsuda & Tanaka, 1997; Steinhardt *et al.*, 1998) based on lower-resolution EM images (∼2 Å) do not generally even approximate correctly the TM distribution. Much better results in this sense are obtained by the HAADF method (resolution of ∼2 Å). Saitoh, Tsuda, Tanaka, Kaneko & Tsai (1997) and Saitoh *et al.* (1998) first found some TM in the AS **B**. The result is remarkable because it was previously assumed that AS **B** contained only Al. They exceed, however, quantitatively, not considering partial and mixed Al/TM occupancy, and especially assuming symmetry 5*m* for AS **B**, while the Al/TM partition reduces the symmetry to 5. In Yan & Pennycook (1999), apart from the observation of different clusters, the improved resolution allowed for the first time to resolve closely spaced TM columns on the outer periphery of the 20 Å diameter cluster. These correspond to TM zigzag chains, suggested by Cockayne & Widom (1998*b*), which we can confirm (*cf.* §2.7). The most recent model (Yan & Pennycook, 2001) determines fairly well many TM positions and the analysis of the situation in the central rings (r < 2.5 Å) is fairly accurate, even though still a bit too simplified. TM in AS **B** (discussed in relation to Saitoh, Tsuda, Tanaka, Kaneko & Tsai, 1997; Saitoh *et al.*, 1998) is neglected; it should be found in the third ring (r = 3.9 Å). Also the number of possible Al sites is too small and fractional/mixed occupancy is neglected outside the first two rings.

Finally, we would like to note that in some works (Saitoh, Tsuda, Tanaka, Kaneko & Tsai, 1997; Saitoh *et al.*, 1998; Yan & Pennycook, 2000) the interpretation of the EM images is aided by considering selected structural features from known approximants (PM phases). This is performed in a proper way, disregarding features which are little compatible with the QC structure (see §1.3.5). The results, accordingly, are quite good. The basic similarity between the *local structure* of QCs and approximants (Steurer, 2001*b*) is also confirmed by our analysis, when due consideration is paid to occupational disorder and to the effects of different TM chemistry.

3.3. The latest structure model

While this manuscript was under review, we learnt of the structure model by Takakura *et al.* (2001). It represents an admirable piece of work, whose only limit is the data set. Performing the data collection by a normal rotating-anode instrument limits the set of observable reflections to those with the highest signal-to-noise ratio. Furthermore, the precision of the data is also smaller. In fact, they used 349 unique reflections ($P10_5/m\,mc$) for refining. Their results are quite good and they mostly compare fairly well with ours. However, due mainly to limitations of the data set, they fail to reveal many interesting details. Another smaller shortcoming is the small extension of the AS's, which introduces systematic errors in the positioning of a minority of sites.

The first macroscopic incongruence in their model is the incorrect value of the crystal density. The value 4.12 Mg m^{-3} is 5% higher than that measured (3.94 ± 2%). We have already discussed (see §2.6.1) how the measured value cannot be underestimated. On the other side, we have also verified that the crystal density is not easily estimated by refinement, owing to correlations. In fact, it has to be constrained to the measured value and the constraint can only be released in the final stages (we put the limit to $wR < 12\%$ on our data set). Takakura *et al.* (2001) used an elastic constraint (a penalty function). This, combined with the limitations of the data set and with the smaller extension of their initial AS's, made obtaining the correct result impossible.

[8] Vertical means along the periodic direction.

There is also a small difference in the samples. Apart from the slightly different composition, their sample does not apparently show an 8 Å modulation.

To compare in a thorough way the two resulting models, we performed a differential refinement with their structure model using our data set (reduced in $P10_5/m\,mc$). The full data set (set II) contains 1544 unique reflections. We also considered the subset (set I) of the 451 reflections with the highest signal-to-noise ratio. The results are listed in Table 5. To account for the possible difference regarding the 8 Å superstructure, we also give separately the values of the statistical indicators (R, wR) restricted to reflections with $h_5 = 0$, which are insensitive to it. Results for our model are reported for comparison. The model of Takakura *et al.* (2001) 'as published' (only scale factor refined) gives results which are even much worse than the published values. To account for the possible variation of sample- and experiment-dependent parameters, we also tried to refine the global parameters, and the static and dynamic ADPs. We proceeded with separate refinements based on sets I and II. It is worth noticing that both refinements end with the same values restricted to set I. However, after refinement based on set I, the statistical indicators on set II are not good. This indicates that set I is too limited to possibly find an accurate structure solution. In every case, however, our model shows a remarkably better quality. As the reflections with $h_5 = 0$ behave quite similarly to the general reflections, we can also say that the effect of the 8 Å modulation is not relevant at this level.

4. Discussion and conclusions

Let us recall an obvious fact: *d*-QC's are three-dimensional. Additional dimensions play the role of order parameters, but the physical reasons for their stability have to be determined in physical space. We have already pointed out (Steurer & Cervellino, 2001) how quasiperiodic planes merge in three dimensions creating oblique net planes. We subscribe to the idea that no substantial physical–structural differences between decagonal and icosahedral phases should exist. In fact, while the electronic transport properties along the periodic axis are very different, due to a slight deformation of the Brillouin zone, mechanical properties also show strong three-dimensional isotropy (Chernikov *et al.*, 1998). The structural relationship with different periodic phases should also be common. We will articulate the discussion on two ordering length scales, for local order (∼20 Å, as the atomic motifs) and for long-range order (the coherence length).

4.1. On the stability of the decagonal phase: local ordering

What can we learn from the structure analysis about the stabilization of *d*-QC's? First of all, consider local ordering. A basic cluster, statistically defined and not exactly unique, does exist and its structure recalls the atomic motifs found in PM phases, with one important difference in the stacking layers (see §§1.3.5 and 2.8). The cluster (columnar) is strongly disordered. This has the effect of increasing the configuration entropy, which in the first approximation[9] we can estimate (see Berthé, 1995, for the algorithm) to be superior to $2\ \mathrm{J\ mol^{-1}\ K^{-1}}$. For comparison, in metallic glasses entropy is typically $R/3 \simeq 2.7\ \mathrm{J\ mol^{-1}\ K^{-1}}$ (Antonione *et al.*, 1990; Garrone & Battezzati, 1985). A compensating effect is to decrease the binding energy, the combined effect being however positive. The high thermodynamic equilibrium temperature accounts for both these effects. Can this kind of local ordering explain the observed ideal quasiperiodic long-range order? Jeong & Steinhardt (1997) explain it in terms of the density of energetically favourable clusters, but the same concept applies equally well to random HBS tilings (Cockayne & Mihalkovič, 1999) and close-packed periodic structures; furthermore, this hypothesis is hard to match with plausible growth mechanisms. Our structure analysis evidences the variability and the disordered nature of the basic cluster; therefore, we cannot imagine a local interaction (the one which holds a cluster together) being responsible for long-range order.

4.2. On the stability of the decagonal phase: long-range order

The cluster(s) structure is very complex and variant. In low resolution (Fig. 6*a*) it appears simpler. This means also that long-wavelength free electrons would 'see' a simpler structure. Free electrons are rarely considered in relation to QCs. Generally, in solid-state physics free electrons are considered to be the ideal mediators of long-range interactions. A long-range electronic contribution to the total energy in QCs has appealing features. In fact, such a term would be compatible with the observed growth and ordering mechanism, because QCs always need long periods of annealing to achieve their best ordered state. QCs as-cast contain a disordered arrangement of clusters, which are stable; these order quasi-periodically only after annealing. Plausibly this electronic long-range energy term (similar to that involved in the modulation of IMS) may step in gradually when passing through an increasing series of LUC approximants, converging on the quasicrystal. This would also explain the phase relationship of QC and LUC approximants (see §1.1.1).

We clarified beyond doubt that the cluster arrangement is ideally quasiperiodic, perhaps a bit more complex than a simple Penrose tiling. The long-range perfect correlation is confirmed by the absence of either phasonic diffuse scattering at the Bragg peak foot or linear phason strain (Abe, Matsuo *et al.*, 2000). It is true that long-range correlation is necessary and not sufficient to infer long-range interactions. However, we can see that short-range ordering is highly imperfect. Therefore, it is difficult to suppose that short-range interatomic interactions *alone* can be the stabilizing force for this structure.

Electron-band effects play a central role in metallic compounds. The Hume–Rothery effect (Mayou, 1994), in

[9] Considering only negative occupancy correlations due to too short distances; positive correlations – Al—TM bonds, TM–TM correlations, recently clarified (Zaharko *et al.*, 2001) – are also present, but not easily quantifiable, so the exact value might be slightly smaller.

particular, seems to be particularly important in intermetallics, either disordered, periodic or quasiperiodic. This effect consists of the creation of pseudogaps at the Fermi energy due to the structural diffraction of electrons. Long-range order plausibly plays a role in this respect, as a pseudogap can be deepened and broadened when the corresponding diffraction peak is sharper and stronger. However, the effect can also be augmented by Al s, p-TM d hybridization (Mayou, 1994) and this is more related to the local coordination (Muller *et al.*, 1998). Remarkably, both PM and VOPAS approximants are generally understood as Hume–Rothery systems (see also §2.9.2). For d-Al–Co–Ni, existing theoretical calculations, which do not confirm the Hume–Rothery effect, of the electronic structure have been based on inadequate models (mainly Burkov's) and the results (Krajčí & Hafner, 1998; Krajčí *et al.*, 2000) are, admittedly, unreliable. From the experimental side, the Hume–Rothery pseudogap has been confirmed for many QCs, d-Al–Co–Ni included (see Belin-Ferré *et al.*, 1996, 2001; Mizutani *et al.*, 2001, and references therein). Isotropic soft X-ray emission/absorption spectroscopy (SXES, SXAS; Belin-Ferré *et al.*, 1996, 2001) confirm a marked pseudogap at the Fermi level in d-Al–Co–Ni. In particular, Al s, p bands are pushed away from the Fermi level on both sides. The shape of the DOS curves also clearly indicates Al s, p–TM d hybridization. The role of the local coordination seems confirmed, together with the effect of long-range order. Little can be said about the extended or localized character of electron states, except what is inferred by the DOS shape comparison. The isotropic averaging mixes periodic and quasiperiodic directions, ruling out comparison. A recent angle-resolved X-ray photoemission study (Rotenberg *et al.*, 2000) on the basic Ni-rich d-Al–Co–Ni phase unequivocably determined the existence of free electron-like s, p bands 3–8.5 eV below the Fermi level, with a broad parabolic dispersion corresponding to an effective mass of 0.9 m_e. This feature holds for both periodic and quasiperiodic directions. Interestingly, the same feature is found – by both experiment and theoretical calculations – in β-AlNi (Muller *et al.*, 1998).

The absence of translational symmetry in three-dimensional space makes it difficult to apply Bloch's theorem to quasiperiodic systems. In periodic systems, Bloch waves are defined as (Ashcroft & Mermin, 1976*b*; Mayou, 1994; Rotenberg *et al.*, 2000)

$$\Psi_{\mathbf{k}}(\mathbf{r}) = u_{\mathbf{k}}(\mathbf{r})\mathrm{e}^{2\pi i\mathbf{kr}} \qquad (1)$$

where $u_{\mathbf{k}}(\mathbf{r})$ is periodic as the direct lattice Λ, hence it can be expanded as a Fourier series on the reciprocal lattice Λ^*

$$u_{\mathbf{k}}(\mathbf{r}) = \sum\nolimits_{\mathbf{h}\in\Lambda^*} c_{\mathbf{k},\mathbf{h}}\mathrm{e}^{2\pi i\mathbf{hr}}. \qquad (2)$$

Quasiperiodic systems can be described as periodic in the embedding space. Then, with a few tricks (as nullifying the kinetic energy in $E^\perp$ by introducing an inverse mass tensor with zero components in $E^\perp$), the above considerations can also be applied to QC. The wavefunctions of (1) shall be interpreted as sections parallel to $E^\perp$, while the moments $\mathbf{k}$, $\mathbf{h}$ shall be projected. However, qualitative interpretation of solutions such as those in (2) is not simple. In fact, the reciprocal lattice Λ^* is dense in physical reciprocal space. This has led to the hypothesis of critically localized waves, in agreement with the picture of QCs as intermediate between periodic and random systems. In the latter, in fact, the reciprocal lattice spreads to a continuum and electrons are strongly localized. However, extended states (or the extended-like character of some critical states) have not been ruled out, especially for three-dimensional QC's (for a short review, see Zijlstra & Janssen, 2000; Maciá, 1999; Rieth & Schreiber, 1998; Huang & Gong, 1998; Kohmoto & Banavar, 1986; Vidal *et al.*, 1999; Avishai & Berend, 1991, and references therein). Another failure of the present theory of QC electrons regards the functional character of the DOS; while the prediction is that of a very spiky DOS, with a dense set of gaps, experiment again (Stadnik *et al.*, 1997; Stadnik, 2001) shows a more traditional absolutely continuous DOS.

Let us try to understand the meaning, in this context, of the QC–VOPAS phase structural relationship. In real QCs, particularly in that presently studied, the intensity distributions on the reciprocal lattice are concentrated in a small subset of strong reflections, with many very weak ones. The refinement of the AS's shows so many partial occupancy subregions because the reflected intensity drops rapidly with increasing length of the scattering vector in perpendicular space. This drop is much faster than what would be for an ideal QC without partial occupancy.[10] The magnitude of the coefficients in (2) is related to the intensity of the relevant Bragg peaks, as far as the pseudopotential magnitude is related to the electron density (Mayou, 1994). This recovers discreteness in the broader meaning of intensity–weighted discreteness. Furthermore, imagine restricting the sum in (2) to the reciprocal lattice Λ^*_{AV} of the PAS, which is an actual discrete subset of the QC's reciprocal lattice (see §A3) with a high relative intensity fraction (see §2.9.1).

We have already pointed out (Steurer & Cervellino, 2001) the importance of two equivalent properties of ideal quasiperiodic order, namely the existence of an average periodic structure (Steurer & Haibach, 1999*b*) and Masáková's binary inflation (see Masáková *et al.*, 2000, and references therein). The latter property seems to be the ideal candidate to replace translational invariance in a reformulation of Bloch's theorem, possibly also developing the concept of 'cluster electrons' put forth by Janot & de Boissieu (1994). Incidentally, this property is only valid for structures having 5-, 8-, 10- or 12-fold axes as noncrystallographic symmetry elements. This covers all the experimentally found quasicrystals and would explain why other exotic symmetries might not be realised.

In conclusion, our structure analysis, beyond the (expected) determination of many common physical and structural features between periodic and aperiodic Al–TM systems, points out the likelihood of a specific, electronic long-range

[10] Note that the fractality of the atomic surfaces, characteristic of random tiling models (de Boissieu *et al.*, 1994), would have the opposite effect, spreading the intensity on higher perpendicular space scattering vectors, resulting in a substantially continuous spectrum rather than a substantially discrete one.

energy term causing long-range ideal aperiodic order. We hope to stimulate a deeper theoretical investigation of this phenomenon.

APPENDIX *A*
Theoretical formalism

A1. Five-dimensional embedding of decagonal quasicrystals

Decagonal quasicrystals can be embedded in a five-dimensional superspace. With respect to the space group, and in particular to the fivefold rotations, this space admits an orthogonal invariant decomposition as a direct sum of the two-dimensional quasiperiodic plane $E^Q\oplus$ the two-dimensional perpendicular (internal) space $E^\perp\oplus$ the one-dimensional decagonal axis E^z. The physical (external, parallel) three-dimensional space $E^{||}$ is the direct sum $E^Q \oplus E^z$. The four-dimensional space E' will be the direct sum of $E^Q \oplus E^\perp$. The arbitrary length scale factor for $E^\perp$ is set to 1. We will use coordinates in a Cartesian reference, or V-basis (Steurer & Haibach, 1999*a*), so $\mathbf{r}_V = (x_1, x_2, x_3, x_4, x_5)_V$, where x_1, x_2 run in E^Q, x_3 in E^z, x_4, x_5 in $E^\perp$.When convenient, we may use the adimensional coordinates

$$\begin{aligned} x &= x_1/a; \\ y &= x_2/a; \\ z &= x_3/c; \\ x^\perp &= x_4/a; \\ y^\perp &= x_5/a, \end{aligned}$$

where a and c are the quasicrystal metric parameters. The coordinates with respect to the five-dimensional unit-cell-defining vectors $\mathbf{d}_i$, $i = 1 \ldots 5$ (D-basis, crystal basis) will be denoted instead by a subscript D. The $\mathbf{d}_i$ vectors in the standard embedding are defined in Steurer & Haibach (1999*a*), equation (3.35). Their V components are the columns of the matrix

$$DV = \frac{a}{5}\begin{vmatrix} -\chi^2 & -\tau^2\chi^2 & -\tau^2\chi^2 & -\chi^2 & 0 \\ \tau\chi & \chi & -\chi & -\tau\chi & 0 \\ 0 & 0 & 0 & 0 & 5c/a \\ -\tau^2\chi^2 & -\chi^2 & -\chi^2 & -\tau^2\chi^2 & 0 \\ -\chi & \tau\chi & -\tau\chi & \chi & 0 \end{vmatrix}, \qquad (3)$$

where $\tau = (1 + 5^{1/2})/2$ is the golden mean (a Pisot number) and $\chi = (3 - \tau)^{1/2}$ is another algebraic (non-Pisot) number, introduced to simplify the notation; they satisfy $\tau^2 - \tau - 1 = 0$, $\chi^4 - 5\chi^2 + 5 = 0$ and $5^{1/2} = \tau\chi^2$. Note that $\mathbf{d}_5 \in E^z$; $E' = E^Q \oplus E^\perp = \text{span}\,(\mathbf{d}_i,\ i = 1 \ldots 4)$. Their lengths and internal angles are $d_j = 2a/5^{1/2}$, $j = 1 \ldots 4$; $d_5 \equiv c$; $\alpha_{ij} = 60^\circ$, $\alpha_{i5} = 90^\circ$, $i, j = 1, \ldots 4$. In the τ^n-embedding, the $\mathbf{d}_i$ can be calculated from the former by the integer-valued matrix S_0^n (see definition in Janner, 1992). This corresponds to multiplying by τ^n their E^Q components, by $(-1/\tau)^n$ their $E^\perp$ components and leaving invariant the E^z component.

The five-dimensional unit-cell volume will be

$$V_c = \left|\det(DV)\right| = 4a^4c(5^{1/2})/25.$$

To determine the atomic coordinates in physical space, we use the concept of atomic surface (AS). An AS is a polytope extended parallel to $E^\perp$, which supports a probability density. The simplest QC models have one AS per five-dimensional unit cell, centred in the origin and with the corresponding site symmetry. In every point where one AS intersects physical space, we will find an atom with a certain probability, which is the corresponding value of the probability density on the AS. The atomic configurations thus obtained reproduce the observed QC Bragg peaks' pattern. Furthermore, every AS (or any of the subregions in which it may be subdivided) is biunivocally associated to a Delone set of (probable) atomic sites.

More complex QC's (as in the present one) have more AS's per unit cell. To keep the diffraction pattern geometry constant, the AS centres must be on a sublattice of the five-dimensional lattice. The most common case is a sublattice of index $5 \times n$ (n being the number of atomic layers per z-translation period). For each atomic layer, consider the four-dimensional section of the unit cell at $x_3 = zc = \text{const}$. Five sublattice nodes are on the fifths of its main body diagonal, with coordinates $(q/5, q/5, q/5, q/5, z)_D$, for $q = 0 \ldots 4$. We will label the AS's by the pair (q, z). The sublattice nodes (and hence the possible AS centres) all belong to the Harker section $(\mathbf{D}, \mathbf{Z})$, $\mathbf{Z}$ denoting the translation period $(0, 0, 0, 0, 1)_D = (0, 0, c, 0, 0)_V$ and $\mathbf{D}$ the four-dimensional diagonal $(1, 1, 1, 1, 0)_D$.

The QC's atomic point density can be simply calculated as (Steurer & Haibach, 1999*a*)

$$n_a = (S_{AS}/V_c) = [5(5^{1/2})S_{\rm AS}]/4a^4c,$$

where $S_{\rm AS}$ is the total area of the atomic surfaces in one unit cell.

A2. Simple tilings and coverings

A2.1. Deterministic tilings. We will henceforth recall a few basic concepts about tilings and coverings, as they are often used for QC structure modelling. We will use their higher-dimensional representation in the above-defined standard embedding. However, as the x_3 coordinate is not important, we will refer to the four-dimensional space obtained by projecting along x_3.

We will particularly discuss Penrose tilings (Penrose, 1974, 1990) in the pentagonal representation ($\text{PPT}^{[m]}$) and in the rhombic representation ($\text{RPT}^{[m]}$). Index m refers to the scaling by τ^m with respect to a fixed reference. Grünbaum & Shepard (1976) can be consulted for the geometric details and relations to other representations of Penrose tilings. Other tiling geometries which deserve discussion are the HBS tiling and the Gummelt decagon covering (GDC). For the discussion it is useful to define the length $a_r = 2a\tau/5$.

$\text{RPT}^{[m]}$ is generated by four pentagonal AS's in $q = 1, 2, 3, 4$. Two of them have radius[11] $a_r\tau^{-m}$, the other two have radius $a_r\tau^{-m-1}$. Details about orientation and disposition

[11] The radius of a regular polygon is its centre-to-vertex distances, or its circumscribed radius, throughout this paper.

of the AS's are found in Steurer & Haibach (1999*a*, 2001). Accordingly, the resulting tiles have edge length $a_r\tau^m$. Two tile shapes (fat rhomb, thin rhomb) are present.

Instead, PPT$^{[n]}$ is generated by a single AS in $q = 0$ (Niizeki, 1989*a*,*b*), having decagonal shape, one vertex of the decagon lying on the x_5 axis. For a decagon radius of $\chi a_r\tau^{-n}$ we have a tile edge length of $\chi a_r\tau^n$. Four tile shapes (pentagon, star, boat, rhomb) are present. These two tilings can be easily mapped onto each other (Grünbaum & Shephard, 1976; Niizeki, 1989*a*,*b*).

Well known is the Gummelt decagon covering GDC$^{[n]}$ (Gummelt, 1996; Jeong & Steinhardt, 1997; Kramer, 1999). The term 'covering' means that the decagonal tiles are allowed to overlap. GDC$^{[n]}$ is composed of decagons of radius $a_r\tau^n$, with one vertex along the x_1 direction from the centre. Two decagons may be in contact, sharing an edge, with centre-to-centre distance $\chi a_r\tau^{n+1}$. Alternatively they overlap in two ways: overlap A, with centre-to-centre distance $\chi a_r\tau^n$; overlap *B*, with centre-to-centre distance $\chi a_r\tau^{n-1}$. The overlap *A* (*B*) distances correspond to the $E^{||}$-projected lengths of the $\mathbf{d}_2$, $\mathbf{d}_3$ ($\mathbf{d}_1$, $\mathbf{d}_4$) vectors, respectively, in the τ^n embedding. The original construction of GDC$^{[n]}$ started from RPT$^{[n-2]}$ (Gummelt, 1996; Kramer, 1999). The centres of the decagons result to form PPT$^{[n]}$ (Gummelt & Bandt, 2000). The frequently observed decagonal clusters in *d*-QC's always have a radius of $\sim$10 Å, corresponding to a value of $n = 3$.

The AS's defining RPT/PPT/GDC can be slightly modified without altering the basic properties of the tiling, only the frequency and distribution of the different tiles will change. An example with a PPT is reported in Niizeki (1993); more general RPT modifications are given in Pavlovitch & Kléman (1987). Of course, the complexity of the pattern will be increasing. However, the number of degrees of freedom (local configurations) remains limited, when and only when the geometric parameters defining the AS's remain limited. We can use this property to define a class of tilings, the general regular pentagonal tilings (GRPTs). This class can be thought of as independent of the chosen geometric representation (set of tiles), provided that a Penrose tiling can be built on it.

A word about the HBS tilings. They constitute one of the many geometric representations of Penrose tiling (Gummelt & Bandt, 2000; Wittmann, 1999; Cockayne & Widom, 1998*b*). However, the HBS representation is very useful to compare *d*-QC's with PM phases (Steurer, 2001*b*). Furthermore, it has attractive properties for the study of random tilings and quasiperiodic dense packing (Gummelt & Bandt, 2000; Cockayne & Mihalkovič, 1999; Cockayne & Widom, 1998*a*).

A2.2. Random tilings. Up to now we have mostly discussed ideal, or deterministic, tilings. These were always possibly defined by a small number of free parameters, *e.g.* those defining the generating AS's. Random tilings (RTs) have been designed for the purpose of increasing the number of statistical degrees of freedom so as to generate large canonical ensembles and consequently a desirably high configurational entropy, by randomizing the spatial disposition of the tiles. Note that this is the only possibility for a tiling meant as a geometric object and also when the atomic decoration of the tiles is constant and deterministic. In real QCs the latter assumptions do not hold, as shown in this work. Consequently, entropy can be effectively introduced on the decoration level. Compare with three-dimensional periodic crystals, where it is more common to have (occupational, chemical, displacive) disorder *in* the unit cell than a disordered arrangement *of* unit cells.

The term 'random tiling' is often used with very broad and different meanings. We shall use a restrictive definition.

First of all, we refer to RT's only in a strict sense (Henley, 1991). In fact, it is improper to refer to RT's in the aforementioned situation, when perfect quasiperiodicity is combined with disorder on the atomic level. These cases are described by a 'well behaved' probability density in the *n*-dimensional unit cell. By 'well behaved' we mean that

(i) the distribution is constant or smoothly variable, or however (piecewise) absolutely continuous, and

(ii) that its support (the set of AS's) is (piecewise) compact and connected.

Secondly, we shall consider RT's only when *quantitatively* necessary. We will *not* refer to RT's in cases that can be seen as a perturbation of an ideally quasiperiodic tiling (de Boissieu *et al.*, 1994). This perturbative effect on Bragg reflection intensities is simply dealt with by the introduction of a phasonic thermal factor, a small width convoluted Gaussian smearing the probability density on the AS's; complementarily, in some cases (Abe, Tamura *et al.*, 2000) weak phasonic diffuse scattering wings around the zone axis of strong Bragg reflections can be observed. Conversely, when this perturbative approach might not hold (Henley *et al.*, 2000), a RT-theoretical approach is convenient.

RTs may be characterized by fractal AS's (de Boissieu *et al.*, 1994) in direct space; however, it is more interesting to characterize them by diffractivity. The diffraction pattern of any object can be divided in absolutely continuous part, singular continuous part and discrete (Bragg) part.[12] It has never been demonstrated that an RT may have a discrete diffraction part (Lagarias, 1999*a*,*b*; Baake & Moody, 1998); they typically show singular continuous diffraction (Tang & Jarić, 1990; Tang, 1990).

A2.3. CsCl-type periodic average structure. The relation between *d*-QC and a CsCl-type PAS is described extensively in Steurer (1999*a*). As physical three-dimensional space $E^{||}$ is the reference for this section, we will keep the notation coherent with the five-dimensional setting, but the ($x4$, $x5$) coordinates (V-basis) will be simply omitted, while the D-basis vectors (hereafter in the standard embedding for simplicity) will be assumed to be projected onto $E^{||}$. The CsCl-type unit cell can be reported to be a *C*-centred orthorhombic setting taking as primitive the vectors [100], [011], [0$\bar{1}$1] of the cubic lattice. By

[12] A robust characterization of Bragg peaks (Landau & Lifshitz, 1960) is the ratio maximum intensity:integral intensity, which increases as $V_{\rm coh}^{2/3}$ ($V_{\rm coh}$ being the coherent volume). Singular continuous spectral features show a much slower increase, or a decrease, of this ratio. While for the first QC's confusion was possible due to very small $V_{\rm coh}$, QC's sample quality is presently on the level of good periodic crystals (Haibach *et al.*, 2000). The spectral characterization is therefore quite solid.

a further slight distortion of the thus obtained orthorhombic cell we obtain the PAS primitive vectors

$$\begin{aligned}\mathbf{a}_{\rm AV} &= (2a/\tau^2)(1,0,0)_V;\\ \mathbf{b}_{\rm AV} &= (2a/\tau\chi)(0,1,0)_V;\\ \mathbf{c}_{\rm AV} &= c(0,0,1)_V,\end{aligned} \tag{4}$$

with $a_{\rm AV}$ = 2.870, $b_{\rm AV}$ = 3.950, $c_{\rm AV} = c$ = 4.0855 Å. The unit-cell volume is V_{AV} = 46.315 Å^3 or $2 \times V_0$, where V_0 is the volume of a cubic cell with lattice parameter a_0 = 2.850 Å. For comparison, the β-AlNi cubic cell has lattice parameter 2.88 Å (Bradley & Taylor, 1937*a*). The reciprocal vectors are

$$\begin{aligned}\mathbf{a}^*_{\rm AV} &= a^*(\tau^2/2,0,0)_V = \tfrac{1}{2}(\bar{1},\bar{2},\bar{2},\bar{1},0)_D;\\ \mathbf{b}^*_{\rm AV} &= a^*(0,\tau\chi/2,0)_V = \tfrac{1}{2}(1,0,0,\bar{1},0)_D;\\ \mathbf{c}^*_{\rm AV} &= c^*(0,0,1)_V = (00001)_D,\end{aligned} \tag{5}$$

as can be easily verified by (3). Due to the reflection condition *hkl*: $h + k = 2n$ for the *C*-centring, the non-extinct part $\Lambda^*_{\rm AV}$ of the PAS reciprocal lattice is a *proper discrete subset* of the ($E^{||}$-projected) *d*-QC reciprocal lattice $\Lambda^*_{\rm QC}$.

The QC's periodic average structure is characterized (in the PAS unit cell) by the average electron density

$$\begin{aligned}\rho_{\rm AV}(\mathbf{r}) &= \lim_{M\to+\infty}\sum_{m,n=-M}^{M}\frac{\rho_{QC}(\mathbf{r}+m\mathbf{a}_{\rm AV}+n\mathbf{b}_{\rm AV})}{(2M+1)^2}\\ &= \rho_{QC}(\mathbf{r}) \star \lim_{M\to+\infty}\sum_{m,n=-M}^{M}\frac{\delta(\mathbf{r}+m\mathbf{a}_{\rm AV}+n\mathbf{b}_{\rm AV})}{(2M+1)^2},\end{aligned} \tag{6}$$

where $\star$ represents convolution. Accordingly, using elementary Fourier transform algebra, it is easy to see that the PAS's structure factors are exactly the subset of the QC's structure factors $F^{\rm QC}_{\mathbf{h}}$ with $\mathbf{h} \in \Lambda^*_{\rm AV} \subset \Lambda^*_{\rm QC}$.

APPENDIX *B*
Acronyms explanation

ADP – atomic displacement parameter
AS – atomic surface
CCAS – cluster-centre-defining atomic surface
EM – electron microscopy
GDC$^{[n]}$ – Gummelt decagon covering (scale τ^n)
HAADF – high-angle annular dark field
HBS – hexagon–boat–star tiling
HRTEM – high-resolution transmission electron microscopy
LUC phase – large unit-cell phase
PAS – periodic average structure
PBP – pentagonal bipyramid
PD – probability density
PM phase – pentagonal motif phase
PPT$^{[n]}$ – pentagonal penrose tiling (scale τ^n)
QC – quasicrystal
RPT$^{[n]}$ – rhombic penrose tiling (scale τ^n)
RT – random tiling
TEM – transmission electrom microscopy
TM – transition metal
VOPAS phase – vacancy-ordered periodic-average-structure phase
XRD – X-ray diffraction

The authors gratefully acknowledge the support of the Swiss National Science Foundation, contract Nos. 20–53630.98 and 2000–06/482.00/1.

References

Abe, E., Saitoh, K., Takakura, K., Tsai, A. P., Steinhardt, P. J. & Jeong, H.-C. (2000). *Phys. Rev. Lett.* **84**, 4609–4612.
Abe, H., Matsuo, Y., Saitoh, H., Kusawake, T., Ohshima, K. & Nakao, H. (2000). *Jpn. J. Appl. Phys. Lett.* **39**, L1111–L1114.
Abe, H., Tamura, N., Le Bolloc'h, D., Moss, S. C., Matsuo, Y., Ishii, Y. & Bai, J. (2000). *Mater. Sci. Eng. A*, **294–296**, 299–302.
Alavi, A., Lozovoi, A. Y. & Finnis, M. W. (1999). *Phys. Rev. Lett.* **82**, 948–951.
Antonione, C., Battezzati, L., Calleri, M. & Marino, F. (1990). *Per. Mineral.* **59**, 121–147.
Ashcroft, N. W. & Mermin, N. D. (1976*a*). *Solid State Physics*, pp. 63–83. Philadelphia: Saunders College.
Ashcroft, N. W. & Mermin, N. D. (1976*b*). *Solid State Physics*, pp. 131–173. Philadelphia: Saunders College.
Avishai, Y. & Berend, D. (1991). *Phys. Rev. B*, **43**, 6873–6879.
Baake, M. & Moody, R. V. (1998). *J. Phys. A*, **31**, 9023–9039.
Bak, P. (1985). *Phys. Rev. B*, **32**, 5764–5772.
Baumgarte, A., Schreuer, J., Estermann, M. A. & Steurer, W. (1997). *Philos. Mag. A*, **75**, 1665–1675.
Becker, P. J. & Coppens, P. (1974*a*). *Acta Cryst.* A**30**, 129–147.
Becker, P. J. & Coppens, P. (1974*b*). *Acta Cryst.* A**30**, 148–153.
Becker, P. J. & Coppens, P. (1975). *Acta Cryst.* A**31**, 417–425.
Belin-Ferré, E., Darkházi, Z., Fournée, V., Sadoc, A., Berger, C., Müller, H. & Kirchmayr, H. (1996). *J. Phys. Condens. Matter*, **8**, 6213–6228.
Belin-Ferré, E., Fournée, V. & Dubois, J. M. (2001). *Mater. Trans. JIM*, **42**, 911–919.
Berthé, V. (1995). *Beyond Quasicrystals*, edited by F. Axel & D. Gratias, pp. 441–463. Les Ulis: Les éditions de physique.
Bester, G., Meyer, B. & Fähnle, M. (1999). *Phys. Rev. B*, **60**, 14492–14495.
Boissieu, M. de, Guyot, P. & Audier, M. (1994). *Lectures on Quasicrystals*, edited by F. Hippert and D. Gratias, pp. 1–152. Les Ulis: Les éditions de physique.
Börnsen, N., Bester, G., Meyer, B. & Fähnle, M. (2000). *J. Alloys Comput.* **308**, 1–14.
Bradley, A. J. & Taylor, A. (1937*a*). *Proc. R. Soc. London A*, **159**, 56–72.
Bradley, A. J. & Taylor, A. (1937*b*). *Philos. Mag.* **23**, 1049–1067.
Burkhardt, U., Ellner, M., Grin, Y. & Baumgartner, B. (1998). *Powd. Diffr.* **13**, 159–162.
Burkov, S. E. (1991). *Phys. Rev. Lett.* **67**, 614–617.
Burkov, S. E. (1993). *Phys. Rev. B*, **47**, 12325–12328.
Cervellino, A. (2001). PhD thesis. ETH, Swiss Federal Institute of Technology, Zurich. http://e-collection.ethbib.ethz.ch/cgi-bin/show.pl?type = diss% nr = 14023.
Cervellino, A., Haibach, T. & Steurer, W. (1998*a*). *Phys. Rev. B*, **57**, 11223–11231.
Cervellino, A., Haibach, T. & Steurer, W. (1998*b*). *Proceedings of the International Conference on Aperiodic Crystals 'Aperiodic'97'*, edited by R. C. M. de Boissieu & J.-L. Verger-Gaugry, pp. 149–153. Singapore: World Scientific.
Cervellino, A., Haibach, T. & Steurer, W. (2000). *Mater. Sci. Eng. A*, **294–296**, 276–278.

Cervellino, A., Haibach, T. & Steurer, W. (2001*a*). *Ferroelectrics*, **250**, 237–240.
Cervellino, A., Haibach, T. & Steurer, W. (2001*b*). In preparation.
Chattopadhyay, K., Lele, S., Thangaraj, N. & Ranganathan, S. (1987). *Acta Metall.* **35**, 727–733.
Chernikov, M. A., Ott, H. R., Bianchi, A., Migliori, A. & Darling, T. W. (1998). *Phys. Rev. Lett.* **80**, 321–324.
Cockayne, E. & Mihalkovič, M. (1999). *Philos. Mag. Lett.* **79**, 441–448.
Cockayne, E. & Widom, M. (1998*a*). *Philos. Mag. A*, **77**, 593–619.
Cockayne, E. & Widom, M. (1998*b*). *Phys. Rev. Lett.* **81**, 598–601.
Deus, C. (1995). Master's thesis. Technische Universität Dresden, Germany.
Dong, C. (1989). *J. Less-Common Met.* **154**, 207–215.
Dong, C., Perrot, A., Dubois, J. M. & Belin, E. (1994). *Mater. Sci. Forum*, **150–151**, 403–416.
Douglas, A. (1950). *Acta Cryst.* **3**, 19–24.
Duneau, M. & Katz, A. (1985). *Phys. Rev. Lett.* **54**, 2688–2691.
Edagawa, K., Echihara, M., Suzuki, K. & Takeuchi, S. (1992). *Philos. Mag. Lett.* **60**, 19–25.
Elcoro, L., Perez-Mato, J. M. & Madariaga, G. (1994). *Acta Cryst.* A**50**, 182–193.
Elcoro, L., Perez-Mato, J. M. & Madariaga, G. (1995). *J. Phys. I Fr.* **5**, 729–745.
Ellner, M., Kek, S. & Predel, B. (1989). *J. Less-Common Met.* **154**, 207–215.
Estermann, M. A., Haibach, T. & Steurer, W. (1994). *Philos. Mag. Lett.* **70**, 379–384.
Estermann, M. A., Lemster, K., Haibach, T. & Steurer, W. (2000). *Z. Kristallogr.* **215**, 584–596.
Freiburg, C., Grushko, B., Wittenberg, R. & Reichert, W. (1996). *Mater. Sci. Forum*, **228–231**, 583–586.
Frey, F., Weidner, E., Hradil, K., Boissieu, M. D., Currat, R., Shibata, K., Tsai, A. P. & Sato, T. J. (2000). *Philos. Mag. A*, **80**, 2375–2392.
Garrone, E. & Battezzati, L. (1985). *Philos. Mag. B*, **52**, 1033–1045.
Gödecke, T. (1997). *Z. Metallkdd.* **88**, 557–569.
Gödecke, T. & Ellner, M. (1996). *Z. Metallkdd.* **87**, 854–864.
Gödecke, T. & Ellner, M. (1997). *Z. Metallkdd.* **88**, 382–389.
Gödecke, T., Scheffer, M., Lück, R., Ritsch, S. & Beeli, C. (1998). *Z. Metallkdd.* **89**, 687–698.
Grin, J., Burkhardt, U., Ellner, M. & Peters, K. (1994*a*). *J. Alloys Comput.* **206**, 243–247.
Grin, J., Burkhardt, U., Ellner, M. & Peters, K. (1994*b*). *Z. Kristallogr.* **209**, 479–487.
Grin, J., Peters, K., Burkhardt, U., Gotzmann, K. & Ellner, M. (1998). *Z. Kristallogr.* **213**, 364–368.
Grünbaum, B. & Shephard, G. C. (1976). *Solid State Physics*, pp. 151–162. Philadelphia: Saunders College.
Grushko, B., Holland-Moritz, D., Wittmann, R. & Wilde, G. (1998). *J. Alloys Comput.* **280**, 215–230.
Gummelt, P. (1996). *Geometriae Dedicata*, **62**, 1–17.
Gummelt, P. & Bandt, C. (2000). *Mater. Sci. Eng. A*, **294–296**, 150–153.
Haibach, T., Cervellino, A., Estermann, M. A. & Steurer, W. (1999). *Philos. Mag. A*, **79**, 933–942.
Haibach, T., Cervellino, A., Estermann, M. A. & Steurer, W. (2000). *Z. Kristallogr.* **215**, 569–583.
Haibach, T., Cervellino, A. & Steurer, W. (1998). *Proc. of the Int. Conf. on Aperiodic Crystals 'Aperiodic'97'*, edited by R. C. M. de Boissieu & J.-L. Verger-Gaugry, pp. 139–148. Singapore: World Scientific.
Haibach, T., Kek, S. & Steurer, W. (1995). *Hasylab Jahresber.* **II**, 417–418.
Haibach, T. & Steurer, W. (1996). *Acta Cryst.* A**52**, 277–286.
Henley, C. L. (1991). *Quasicrystals: The State of the Art*, edited by D. P. DiVincenzo & P. J. Steinhardt, pp. 429–524. Singapore: World Scientific.
Henley, C. L., Elser, V. & Mihalkovič, M. (2000). *Z. Kristallogr.* **215**, 553–568.
Hiraga, K., Lincoln, F. J. & Sun, W. (1991). *Mater. Trans. JIM*, **32**, 308–312.
Hiraga, K., Ohsuna, T. & Nishimura, S. (2000). *Philos. Mag. Lett.* **80**, 653–659.
Hiraga, K., Ohsuna, T. & Nishimura, S. (2001). *Philos. Mag. Lett.* **81**, 109–115.
Hiraga, K., Sun, W. & Yamamoto, A. (1994). *Mater. Trans. JIM*, **35**, 657–662.
Honal, M., Haibach, T. & Steurer, W. (1998). *Acta Cryst.* A**54**, 374–387.
Hory, R., Pohla, C. & Ryder, P. L. (1999). *Philos. Mag. A*, **79**, 549–560.
Huang, X. & Gong, C. (1998). *Phys. Rev. B*, **58**, 739–744.
Hudd, R. C. & Taylor, W. (1962). *Acta Cryst.* **15**, 441–442.
Janner, A. (1992). *Acta Cryst.* A**48**, 884–901.
Janot, C. & de Boissieu, M. (1994). *Phys. Rev. Lett.* **72**, 1674–1677.
Janssen, T. (1986). *Acta Cryst.* A**42**, 261–271.
Jeong, H.-C. & Steinhardt, P. J. (1997). *Phys. Rev. B*, **55**, 3520–3532.
Joseph, D., Ritsch, S. & Beeli, C. (1997). *Phys. Rev. B*, **55**, 8175–8183.
Kalning, M., Kek, S., Burandt, B., Press, W. & Steurer, W. (1994). *J. Phys. Condens. Matter*, **6**, 6177–6187.
Kalning, M., Kek, S., Krane, H. G., Dorna, V., Press, W. & Steurer, W. (1997). *Phys. Rev. B*, **55**, 187–192.
Kalning, M., Press, W. & Kek, S. (1995). *Philos. Mag. Lett.* **71**, 341–349.
Kalugin, P., Kitaev, A. Y. & Levitov, L. S. (1985). *JETP Lett.* **41**, 145–149.
Kalugin, P. & Levitov, L. (1989). *Int. J. Mod. Phys. B*, **3**, 877–896.
Kanazawa I., Hamada, E., Saeki, T., Sato, K., Nakata, M., Takeuchi, S. & Wollgarten, M. (1997). *Phys. Rev. Lett.* **79**, 2269–2272.
Kanazawa, I., Nakayama, C., Takahashi, Y., Ohata, T., Iwashita, T. & Kizuka, T. (1994). *Phys. Rev. B*, **49**, 3573–3575.
Katz, A. & Gratias, D. (1994). *Lectures on Quasicrystals*, edited by F. Hippert & D. Gratias, pp. 187–264. Les Ulis: Les éditions de physique.
Kohmoto, M. & Banavar, J. R. (1986). *Phys. Rev. B*, **34**, 563–566.
Korzhavyi, P. A., Ruban, A. V., Lozovoi, A. Y., Vekilov, Y. K., Abrikosov, I. A. & Johansson, B. (1999). *Phys. Rev. Lett.* **83**, 979–982.
Krajčí, M. & Hafner, J. (1998). *Phys. Rev. B*, **58**, 5378–5383.
Krajčí, M., Hafner, J. & Mihalkovič, M. (2000). *Phys. Rev. B*, **62**, 243–255.
Kramer, P. (1999). *J. Phys. A*, **32**, 5781–5793.
Lagarias, J. C. (1999*a*). *Discrete Comput. Geom.* **21**, 161–191.
Lagarias, J. C. (1999*b*). *Discrete Comput. Geom.* **21**, 345–372.
Landau, L. D. & Lifshitz, E. M. (1960). *Course of Theoretical Physics*, Vol. 8, translated by J. B. Sykes & J. S. Bell. Oxford: Pergamon Press.
Lawther, D. W. & Dunlap, R. A. (1994). *Phys. Rev. B*, **49**, 3183–3189.
Lemster, K. (2001). PhD thesis. ETH, Swiss Federal Institute of Technology, Zurich. http://e-collection.ethbib.ethz.ch/cgi-bin/show.pl?type = diss% nr = 14141.
Li, X. Z., Shi, N. C., Ma, Z. S., Ma, X. L. & Kuo, K. H. (1995). *Philos. Mag. Lett.* **72**, 79–86.
Li, X. Z., Steurer, W., Haibach, T., Zhang, B. & Frey, P. (1995). *Z. Kristallogr.* **210**, 509–512.
Lück, R. (2000). *Mater. Sci. Eng. A*, **294–296**, 263–267.
Ma, X. L. & Kuo, K. H. (1994). *Metall. Mater. Trans. A*, **25**, 47–56.
Ma, X. L., Li, X. Z. & Kuo, K. H. (1995). *Acta Cryst.* B**51**, 36–43.
Maciá, E. (1999). *Phys. Rev. B*, **60**, 10032–10036.
Mancini, L., Janot, C., Loreto, L., Farinato, R., Gastaldi, J. & Baruchel, J. (1998). *Philos. Mag. Lett.* **78**, 159–167.
Mandal, R. K. & Lele, S. (2000). *Mater. Sci. Eng. A*, **294–296**, 366–368.
Masáková, Z., Pelantová, E. & Svobodová, M. (2000). *Lett. Math. Phys.* **54**, 1–10.
Mayou, D. (1994). *Lectures on Quasicrystals*, edited by F. Hippert & D. Gratias, pp. 417–462. Les Ulis: Les éditions de physique.

Mihalkovič, M., Elhor, H. & Suck, J.-B. (2001). *Phys. Rev. B*, 214301:1–14.
Mizutani, U., Takeuchi, T., Fournée, V., Sato, H., Banno, E. & Onogi, T. (2001). *Scr. Mater.* **44**, 1181–1185.
Muller, D. A., Singh, D. J. & Silcox, J. (1998). *Phys. Rev. B*, **57**, 8181–8202.
Nakao, Y., Shibuya, T., Takeuchi, S., Liu, W., Li, X.-S. & Berko, S. (1992). *Phys. Rev. B*, **46**, 3108–3111.
Nakao, Y., Shibuya, T., Takeuchi, S., Liu, W., Li, X.-S. & Berko, S. (1993). *Phys. Rev. B*, **48**, 3030–3036.
Niizeki, K. (1989*a*). *J. Phys. A*, **22**, 4281–4293.
Niizeki, K. (1989*b*). *J. Phys. A*, **22**, 193–204.
Niizeki, K. (1993). *Mater. Trans. JIM*, **34**, 109–115.
Ohata, T., Kanazawa, I., Iwashita, T., Kishi, K. & Takeuchi, S. (1990). *Phys. Rev. B*, **42**, 6730–6732.
Pavlovitch, A. & Kléman, M. (1987). *J. Phys. A*, **20**, 687–702.
Penrose, A. (1974). *Bull. Inst. Maths. Appl.* **10**, 266–271.
Penrose, R. (1990). *Per. Mineral.* **59**, 95–100.
Prekul, A. F., Kazanstev, V. A., Shalaeva, E. V. & Shchegolikhina, N. I. (1998). *JETP Lett.* **67**, 203–209.
Rabson, D. A., Mermin, N. D., Rokhsar, D. S. & Wright, D. C. (1991). *Rev. Mod. Phys.* **63**, 699–733.
Rieth, T. & Schreiber, M. (1998). *J. Phys.* **10**, 783–800.
Ritsch, S., Beeli, C., Lück, R. & Hiraga, K. (1999). *Philos. Mag. Lett.* **79**, 225–232.
Ritsch, S., Beeli, C., Nissen, H.-U., Gödecke, T., Scheffer, M. & Lück, R. (1996). *Philos. Mag. Lett.* **74**, 99–106.
Ritsch, S., Beeli, C., Nissen, H.-U., Gödecke, T., Scheffer, M. & Lück, R. (1998). *Philos. Mag. Lett.* **78**, 67–75.
Ritsch, S. L. (1996). PhD Thesis. ETH, Swiss Federal Institute of Technology, Zurich.
Rotenberg, E., Theis, W., Horn, P. & Gille, K. (2000). *Nature*, **406**, 602–605.
Saitoh, K., Tsuda, K. & Tanaka, M. (1997). *Philos. Mag. A*, **76**, 135–150.
Saitoh, K., Tsuda, K. & Tanaka, M. (1998). *J. Phys. Soc. Jpn. Lett.* **67**, 2578–2581.
Saitoh, K., Tsuda, K., Tanaka, M., Kaneko, K. & Tsai, A. P. (1997). *Jpn. J. Appl. Phys. Lett.* **37**, L1400–L1402.
Saitoh, K., Tsuda, K., Tanaka, M. & Tsai, A. P. (1999). *Jpn. J. Appl. Phys. Lett.* **38**, L671–L674.
Saitoh, K., Tsuda, K., Tanaka, M., Tsai, A. P., Inoue, A. & Matsumoto, T. (1994). *Mater. Sci. Eng. A*, **182**, 805–810.
Saitoh, K., Yokosawa, T., Tanaka, M. & Tsai, A. P. (1999). *J. Phys. Soc. Jpn. Lett.* **68**, 2886–2889.
Sato, K., Takahashi, Y., Uchiyama, H., Kanazawa, I., Tamura, R., Kimura, K., Komori, F., Suzuki, R., Ohdaira, T. & Takeuchi, S. (1999). *Phys. Rev. B*, **59**, 6712–6716.
Schapink, F. W. (2001). *Philos. Mag. A*, **81**, 883–901.
Scheffer, M., Gödecke, T., Lück, R., Ritsch, S. & Beeli, C. (1998). *Z. Metallkdd.* **89**, 270–278.
Stadnik, Z. M. (2001). *Mater. Trans. JIM*, **42**, 920–927.
Stadnik, Z. M., Purdie, D., Garnier, M., Baer, Y., Tsai, A.-P., Inoue, A., Edagawa, K., Takeuchi, S. & Buschow, K. H. J. (1997). *Phys. Rev. B*, **55**, 10938–10951.
Steinhardt, P. J., Jeong, H.-C., Saitoh, K., Tanaka, M., Abe, E. & Tsai, A. P. (1998). *Nature*, **396**, 55–57.
Steurer, W. (1990). *Z. Kristallogr.* **190**, 179–234.
Steurer, W. (1999*a*). *Proc. of the Int. Conf. on Solid–Solid Phase Transformations '99 (JIMIC-3)*, edited by K. O. M. Koiwa & T. Miyazaki, pp. 1333–1336. Tokyo: The Japan Institute of Metals.
Steurer, (1999*b*). *MRS Symp. Proc. – Quasicrystals*, edited by A. P. T. J. M. Dubois, P. A. Thiel & K. Urban, Vol. 553, pp. 159–170. Warrensdale: Materials Research Society.
Steurer, W. (2000). *Z. Kristallogr.* **215**, 323–334.
Steurer, W. (2001*a*). *MRS Symp. Proc. – Quasicrystals*, edited by A. P. Tsai, E. Beli-Ferré, P. A. Thiel & K. Urban, Vol. 643. In the press. Warrensdale: Materials Research Society.
Steurer, W. (2001*b*). *Ferroelectrics*, **250**, 377–380.
Steurer, W. & Cervellino, A. (2001). *Acta Cryst.* A**57**, 333–340.
Steurer, W. & Frey, F. (1993). *J. Non-Cryst. Solids*, **153**, 600–605.
Steurer, W. & Frey, F. (1998). *Phase. Transit.* **67**, 319–361.
Steurer, W. & Haibach, T. (1999*a*). *The Physics of Quasicrystals*, edited by Z. M. Stadnik, pp. 51–89. Heidelberg: Springer.
Steurer, W. & Haibach, T. (1999*b*). *Acta Cryst.* A**55**, 48–57.
Steurer, W. & Haibach, T. (2001). *International Tables for Crystallography*, edited by U. Shmueli, 2nd ed., pp. 486–532. Dordrecht: Kluwer Academic Publishersss.
Steurer, W., Haibach, T., Zhang, B., Kek, S. & Lück, R. (1993). *Acta Cryst.* B**49**, 661–675.
Steurer, W. & Kuo, K. H. (1990). *Acta Cryst.* B**46**, 703–712.
Takakura, H., Yamamoto, A. & Tsai, A. P. (2001). *Acta Cryst.* A**57**, 576–585.
Tang, L.-H. (1990). *Phys. Rev. Lett.* **64**, 2390–2393.
Tang, L.-H. & Jarić, M. V. (1990). *Phys. Rev. B*, **41**, 4524–4546.
Thornley, F. R. (1983). *Acta Cryst.* A**39**, 326–332.
Thornley, F. R. & Nelmes, R. J. (1974). *Acta Cryst.* A**30**, 748–757.
Tsai, A. P., Inoue, A. & Matsumoto, T. (1989). *Mater. Trans. JIM*, **30**, 463–473.
Tsuda, K., Nishida, Y., Saitoh, K., Tanaka, M., Tsai, A. P., Inoue, A. & Matsumoto, T. (1996). *Philos. Mag. A*, **74**, 697–708.
Vidal, J., Mouhanna, D. & Gianmarchi, T. (1999). *Phys. Rev. Lett.* **83**, 3908–3911.
Villars, P. & Calvert, L. D. (1991). *Pearson's Handbook of Crystallographic Data for Intermetallic Phases.* Ohio, USA: ASM International.
Welberry, T. R. (1985). *Rep. Prog. Phys.* **48**, 1543–1594.
Wittmann, R. (1999). *Z. Kristallogr.* **214**, 501–505.
Würschum, R., Grushko, B., Urban, K. & Schaefer, H.-E. (1994). *Philos. Mag. B*, **70**, 913–917.
Würschum, R., Troev, T. & Grushko, B. (1995). *Phys. Rev. B*, **52**, 6411–6416.
Yamamoto, A. (1996). *Sci. Rep. Res. Inst. Tohoku University A*, **42**, 207–212.
Yamamoto, A., Kato, K., Shibuya, T. & Takeuchi, S. (1990). *Phys. Rev. Lett.* **65**, 1603–1606.
Yamamoto, K., Jono, M. & Matsuo, Y. (1999). *J. Phys. Condens. Matter*, **11**, 1015–1026.
Yan, Y. & Pennycook, S. J. (1999). *Nature*, **403**, 266–267.
Yan, Y. & Pennycook, S. J. (2000). *Phys. Rev. B*, **61**, 14291–14294.
Yan, Y. & Pennycook, S. J. (2001). *Phys. Rev. Lett.* **86**, 1542–1545.
Yan, Y., Pennycook, S. J. & Tsai, A. P. (1998). *Phys. Rev. Lett.* **81**, 5145–5148.
Zaharko, O., Meneghini, C., Cervellino, A. & Fischer, E. (2001). *Eur. Phys. J.* **19**, 207–214.
Zeger, G., Plachke, D., Carstanjen, H. D. & Trebin, H.-R. (1999). *Phys. Rev. Lett.* **82**, 5273–5276.
Zhang, B. (1995). PhD Thesis. ETH, Swiss Federal Institute of Technology, Zurich.
Zhang, B., Estermann, M. A. & Steurer, W. (1995). *Z. Kristallogr.* Suppl. 10, 120.
Zhang, B., Estermann, M. A. & Steurer, W. (1997). *J. Mater. Res.* **12**, 2274–2280.
Zhang, B., Gramlich, V. & Steurer, W. (1995). *Z. Kristallogr.* **210**, 498–503.
Zhang, L. M., Dong, C., Brunet, P. & Dubois, J. M. (2000). *Mater. Sci. Eng. A*, **294–296**, 810–812.
Zijlstra, E. S. & Janssen, T. (2000). *Phys. Rev. B*, **61**, 3377–3383.
Zurkirch, M., Bolliger, B., Erbudak, M. & Kortan, A. R. (1998). *Phys. Rev. B*, **58**, 14113–14116.